

A STABILIZED ARBITRARY LAGRANGIAN–EULERIAN SLIDING INTERFACE METHOD FOR FLUID-STRUCTURE INTERACTION WITH A ROTATING RIGID STRUCTURE *

YALI GAO[†], JIASHUN HU[‡], AND BUYANG LI[§]

Abstract. We introduce a novel sliding interface formulation for fluid-structure interaction (FSI) between a rotating rigid structure and incompressible fluid, improving existing methodologies with a skew-symmetric Nitsche’s stabilization term applied on an artificial sliding interface, alongside a rotational arbitrary Lagrangian-Eulerian framework. This innovative approach not only preserves the energy-dissipating property at the continuous level but also provides a robust foundation for further advancements in FSI modeling. Our methodology includes a first-order full discretization that maintains these critical energy-dissipating properties at the discrete level, ensuring numerical stability and accuracy. While prior contributions such as the original sliding interface method introduced by Bazilevs & Hughes (Comput. Mech., 43(1):143–150, 2008) have been significant, theoretical analyses such as the inf-sup condition on non-matching meshes have gone largely unaddressed. We fill this gap by proving the inf-sup condition within the context of the isoparametric finite element method (FEM), where meshes are not only non-matching but also overlapping, thus extending the applicability and robustness of our approach. Leveraging this inf-sup condition along with the inherent energy-dissipating properties, we establish the unique solvability of the fully discrete scheme. Through extensive numerical experiments, we illustrate the convergence, efficiency, and energy-dissipating property of the proposed method.

Key words. Fluid-structure interaction, sliding interface method, arbitrary Lagrangian-Eulerian, Nitsche’s method, finite element method, energy dissipation

AMS subject classifications. 65M60, 65N12, 74F10, 76D05, 76U05

1. Introduction. The fluid-structure interaction (FSI) problem is a major challenge in computational fluid dynamics, with applications in geophysics, bioengineering, and hydrodynamics [15, 16, 21, 25–27]. In recent decades, simulating FSI with rotating structures has become increasingly important due to industrial and engineering demands, such as in the design and analysis of wind turbines [5–7], ship propellers [9], jet engines [26], and artificial heart pumps [29]. The presence of rotating bodies adds complexity to the problem due to the significantly changing fluid domain. Developing stable and accurate schemes for FSI involving rotating structures is crucial for advancing these applications.

In this paper, we consider the interaction between the incompressible fluid and a rigid structure which spins around a rigid axis, see Fig. 1.1a. Mathematically, the motion of the fluid can be described by the incompressible Navier-Stokes equations in a moving domain $\Omega(t) \subset \mathbb{R}^d$, $d = 2, 3$,

$$\rho_f(\partial_t \mathbf{u} + \mathbf{u} \cdot \nabla \mathbf{u}) - \nabla \cdot \boldsymbol{\sigma}(\mathbf{u}, p) = \rho_f \mathbf{f} \quad \text{in } \bigcup_{t \in (0, T]} \Omega(t) \times \{t\}, \quad (1.1a)$$

$$\nabla \cdot \mathbf{u} = 0 \quad \text{in } \bigcup_{t \in (0, T]} \Omega(t) \times \{t\}, \quad (1.1b)$$

where $\boldsymbol{\sigma}(\mathbf{u}, p) = 2\mu \mathbb{D}(\mathbf{u}) - p\mathbb{I}$ denotes the stress tensor, $\mathbb{D}(\mathbf{u}) = \frac{1}{2}(\nabla \mathbf{u} + (\nabla \mathbf{u})^T)$ the

*Y. Gao is supported by the NSFC, PR China (No. 12371406), Young Talent Fund of Xi’an Association for Science and Technology (No. 959202413091), Shaanxi Fundamental Science Research Project for Mathematics and Physics (No. 23JSQ030). J. Hu is supported in part by the CAS AMSS-PolyU Joint Laboratory of Applied Mathematics and the Hong Kong Research Grants Council (GRF project no. 15301321). B. Li is supported in part by the Hong Kong Research Grants Council (RFS2324-5S03) and The Hong Kong Polytechnic University (project ID: P0051154).

[†]Department of Applied Mathematics, Northwestern Polytechnical University, Xi’an Shanxi, China. E-mail address: gaoylimath@nwpu.edu.cn

[‡]Department of Applied Mathematics, The Hong Kong Polytechnic University, Hong Kong. E-mail address: jiashun.hu@polyu.edu.hk

[§]Department of Applied Mathematics, The Hong Kong Polytechnic University, Hong Kong. E-mail address: buyang.li@polyu.edu.hk

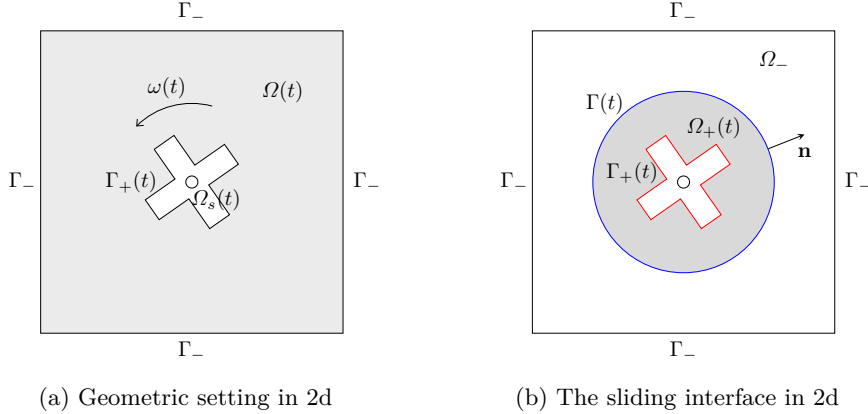


Fig. 1.1: Geometric setting and the sliding interface

deformation matrix and \mathbb{I} the identity matrix. ρ_f and μ denote the density and the viscosity of the fluid. The moving domain $\Omega(t)$ is enclosed by a fixed boundary Γ_- and the rotating interface $\Gamma_+(t)$ which is the boundary of the rigid structure part. According to the rigid property, the motion of the structure part is described by its angular speed $\omega(t)$. These two systems are coupled together by non-slip boundary conditions and force balance at the interface $\Gamma_+(t)$. Thus, the fluid velocity needs to satisfy the following boundary conditions,

$$\mathbf{u} = \omega(t)\mathbf{v}_{\Gamma_+(t)} \quad \text{on } \bigcup_{t \in (0, T]} \Gamma_+(t) \times \{t\}, \quad (1.1c)$$

$$\mathbf{u} = 0 \quad \text{on } \Gamma_-, \quad (1.1d)$$

where \mathbf{v}_{Γ_+} denotes the rotating velocity field on Γ_+ with unit angular speed. Moreover, the rigid structure's angular momentum changes at a rate equal to the torque exerted by the fluid,

$$I_s \omega'(t) = \rho_f \int_{\Gamma_+(t)} (\boldsymbol{\sigma}(\mathbf{u}, p) \cdot \mathbf{n}_s) \cdot \mathbf{v}_{\Gamma_+}, \quad (1.1e)$$

where I_s is a constant that denotes the moment of inertia of $\Omega_s(t)$ and \mathbf{n}_s denotes the exterior normal of $\Omega_s(t)$. We can compare the coupled system (1.1) with two related problems, namely, the Dirichlet problem of Navier-Stokes equations on a moving domain with rotating and stationary boundaries and the FSI with a rotating elastic structure. Their common feature is that the fluid region exhibits significant but regular deformation. In contrast, (1.1) simplifies the elastic response of the structure while preserving the energy-dissipation property in the absence of external forces, i.e., when $\mathbf{f} = 0$:

$$\frac{d}{dt} E(t) \leq 0, \quad E(t) = \frac{1}{2} \int_{\Omega(t)} |\mathbf{u}|^2 dx + \frac{1}{2} I_s \omega(t)^2. \quad (1.2)$$

The Dirichlet problem of Navier-Stokes equations on a rotating domain, on the other hand, does not exhibit similar energy-dissipation property due to the Dirichlet boundary conditions applied at the rotating boundary. Designing numerical schemes that respect the energy-dissipation law (1.2) of the coupled system (1.1) can be challenging and serve as a fundamental step for developing more sophisticated energy-dissipating methods for systems involving rotating elastic structures.

One of the most popular methods for solving the FSI problem is the arbitrary Lagrangian-Eulerian (ALE) finite element method (FEM) introduced by Formaggia & Nobile [19]. In this approach, the fluid mesh moves with a mesh velocity \mathbf{w}_h to accommodate the defor-

mations of the structure interface [1, 12, 22, 27, 28]. However, as one of the main features of (1.1), the conflict between the rotating interface and the stationary exterior boundary of the fluid prevents the direct application of the ALE method. The essential reason is that the ALE method keeps the mesh connectivity, which makes the distortion of the fluid mesh inevitable unless some computationally expensive re-meshing procedures are performed.

Many approaches have been proposed to solve the mesh distortion issue caused by a rotating boundary. Popular solutions include the shear-slip mesh update method (SSMUM) [5, 6, 8, 10, 30, 31], the sliding interface method [9], and the modified ALE method [21, 23, 29, 33]. A common feature of these methods is the usage of an artificial cylindrical interface. This artificial interface encloses the rotating structure and confines the fluid domain deformation within it, while maintaining a fixed mesh outside. By exploiting the symmetric properties of the cylindrical interface, the SSMUM performs an efficient remeshing procedure by reconnecting nodes only in a single layer of elements closest to the interface. To handle the sudden change of the finite element (FE) spaces, the SSMUM is usually implemented in the space-time FEM framework, which allows solutions at different time steps to be in different FE spaces, and enforces the continuity weakly by Nitsche's method. In contrast, the modified ALE method regards the mesh updating procedure as the result of applying some mesh velocity, allowing the use of the ALE framework instead of space-time FEM. However, from the ALE perspective, the magnitude of the resulting mesh velocity is of order $\mathcal{O}(h\tau^{-1})$ on the cylindrical interface, which can lead to an infinite velocity for semi-discrete problem $\tau \rightarrow 0$ and pose difficulty for the error analysis of the modified ALE method. Moreover, the sudden change of the finite element spaces makes it difficult to develop energy-dissipating schemes, and strong CFL conditions are needed for designing stable schemes in the above two approaches.

Comparatively, the sliding interface approach avoids sudden mesh changes, making it a more promising option for designing numerical schemes with unconditional stability and energy-dissipating properties. As demonstrated in Fig. 1.1b, the artificial interface $\Gamma(t)$ splits the moving domain into two subdomains: a rotating interior domain $\Omega_+(t)$ and a stationary domain Ω_- . The approach proposed in [9] decomposed the Navier-Stokes equations on $\Omega(t)$ into subproblems, applied the ALE method on the rotating subdomain, and coupled them together by weakly enforcing the continuity conditions on the artificial cylindrical interface. Following the idea of interior penalty upwind discontinuous Galerkin method (SIPG), penalty terms are added on the artificial cylindrical interface to enhance the stability of the method. Denoting the solutions on subdomains as \mathbf{u}_\pm and p_\pm , and test functions as \mathbf{v}_\pm and q_\pm , the discontinuity of test functions leads to the consistency term in the weak form

$$-\frac{1}{2} \int_{\Gamma} (\mathbf{v}_+ - \mathbf{v}_-) (\boldsymbol{\sigma}(\mathbf{u}_+, p_+) \cdot \mathbf{n} + \boldsymbol{\sigma}(\mathbf{u}_-, p_-) \cdot \mathbf{n}), \quad (1.3)$$

in which the continuity of the normal stress is also weakly imposed and \mathbf{n} denotes the unit normal on $\Gamma(t)$ pointing into $\Omega_-(t)$. To stabilize this interfacial term, a skew-symmetric penalty term in pressure and a symmetric penalty term in velocity are considered,

$$-\frac{1}{2} \int_{\Gamma} (\mathbf{u}_+ - \mathbf{u}_-) (q_+ \cdot \mathbf{n} + q_- \cdot \mathbf{n}) - \frac{1}{2} \int_{\Gamma} (\mathbf{u}_+ - \mathbf{u}_-) (2\mu \mathbb{D} \mathbf{v}_+ \cdot \mathbf{n} + 2\mu \mathbb{D} \mathbf{v}_- \cdot \mathbf{n}). \quad (1.4)$$

Finally, the convection term $(\mathbf{u} \cdot \nabla \mathbf{u}, \mathbf{v})$ is stabilized by including an upwind stabilization in the penalty term, i.e.,

$$-\int_{\Gamma} (\mathbf{u}_+ - \mathbf{u}_-) (\mathbf{v}_+ - \mathbf{v}_-) (\text{neg}(\mathbf{u}_+ \cdot \mathbf{n}) + \text{neg}(-\mathbf{u}_- \cdot \mathbf{n})), \quad (1.5)$$

where $\text{neg}(a) = \min\{0, a\}$ denotes the negative part. As a result, the subdomain problems can be solved using different meshes: the interior mesh rotates with the structure, allowing the application of the ALE method, while the exterior mesh remains fixed. However, the mismatch in meshes, velocities, and pressures across the sliding interface introduces

significant challenges in designing a solvable, energy-dissipating scheme. The first challenge is proving the inf-sup condition on the non-matching meshes, which is crucial for the scheme's solvability. This theoretical issue was left unresolved in [9]. Additionally, this paper uses isoparametric FEM instead of isogeometric analysis for spatial discretization, which adds complexity due to the potential overlap of the non-matching sub-meshes. The second challenge is to preserve the energy-dissipation property, which requires a careful selection of interfacial penalty terms for both the velocity and the pressure. Furthermore, the involvement of ALE velocity introduces additional difficulties in designing a fully discrete, energy-dissipating scheme, as discussed in [18, 20] for two-phase flows. To the best of our knowledge, no fully discrete scheme for the FSI problem with a rotating rigid structure, whether based on the SSMUM framework or the sliding interface method, has successfully preserved the energy-dissipation property.

The main contribution of this paper is to propose a fully discrete energy-dissipating sliding interface method for (1.1), using isoparametric FEM for spatial discretization. There are two main obstacles to overcome: the penalty terms on the artificial interface, which are present at the continuous level, and the effect of the ALE velocity on energy dissipation, which must be carefully addressed during discretization. For the first issue, we replace (1.4) by a skew-symmetric penalty term in both pressure and velocity,

$$\frac{1}{2} \int_{\Gamma} (\mathbf{u}_+ - \mathbf{u}_-) (\boldsymbol{\sigma}(\mathbf{v}_+, q_+) \cdot \mathbf{n} + \boldsymbol{\sigma}(\mathbf{v}_-, q_-) \cdot \mathbf{n}),$$

which shares similarity with the discontinuous finite element methods applied to convection-diffusion problems and the Navier-Stokes equations, as discussed in [3, 4]. Moreover, the convection term is reformulated into the skew-symmetric form with additional boundary terms by integration by parts, see also [2, 18, 20],

$$(\mathbf{z} \cdot \nabla \mathbf{u}, \mathbf{v})_{\Omega_i} + \frac{1}{2} ((\nabla \cdot \mathbf{z}) \mathbf{u}, \mathbf{v})_{\Omega_i} = b_i(\mathbf{z}; \mathbf{u}, \mathbf{v}) + \frac{1}{2} \int_{\partial \Omega_i} (\mathbf{z} \cdot \mathbf{n}_i) \mathbf{u} \cdot \mathbf{v} dA, \quad (1.6)$$

where \mathbf{n}_i represents the exterior normal of Ω_i , dA denotes the surface measure on $\partial \Omega_i$, $i = \pm$, $b_i(\mathbf{z}; \mathbf{u}, \mathbf{v})$ is trilinear and skew-symmetric with respect to \mathbf{u} and \mathbf{v} ,

$$b_i(\mathbf{z}; \mathbf{u}, \mathbf{v}) = \frac{1}{2} (\mathbf{z} \cdot \nabla \mathbf{u}, \mathbf{v})_{\Omega_i} - \frac{1}{2} (\mathbf{z} \cdot \nabla \mathbf{v}, \mathbf{u})_{\Omega_i}. \quad (1.7)$$

The convection terms of the subproblems correspond to $\mathbf{z} = \mathbf{u}_+ - \mathbf{w}_+$ and $\mathbf{z} = \mathbf{u}_-$, respectively, where \mathbf{w}_+ denotes the ALE mesh velocity inside the rotating subdomain. Using $\mathbf{u}_+ = \mathbf{u}_-$ on Γ , the boundary terms in (1.6) on the cylindrical interface Γ write

$$\frac{1}{2} \int_{\Gamma} \frac{1}{2} \left((\mathbf{u}_+ \cdot \mathbf{n}) \mathbf{u}_+ + (\mathbf{u}_- \cdot \mathbf{n}) \mathbf{u}_- \right) \cdot (\mathbf{v}_+ - \mathbf{v}_-) - \frac{1}{2} \int_{\Gamma} (\mathbf{w}_+ \cdot \mathbf{n}) \mathbf{u}_+ \cdot \mathbf{v}_+.$$

The first term is again stabilized in a skew-symmetric way by utilizing $\mathbf{u}_+ = \mathbf{u}_-$ on Γ , while the second term poses the only requirement on the ALE velocity: $\mathbf{w}_+ \cdot \mathbf{n} = 0$ on Γ . Since the ALE mesh rotates to fit $\Gamma_+(t)$, according to (1.1c), the above requirement can be fulfilled by choosing \mathbf{w}_+ as a rotational velocity field on Γ . In this way, we derive the equivalent energy-dissipating weak formulation for (1.1) in the continuous form with a moving ALE frame on the rotating subdomain (see Lemma 2.1). To preserve the energy-dissipation law at the fully discrete level, the treatment of the term $\nabla \cdot \mathbf{w}_+$ on the left side of (1.6) is essential. The case where \mathbf{w}_+ is divergence free is simpler and can be treated following the idea of [18]. The general case where $\nabla \cdot \mathbf{w}_+ \neq 0$ is more difficult and frequently encountered in applications such as the FSI with an elastic structure and the Navier-Stokes equations on moving domains with the Dirichlet boundary condition. In the latter case, we apply the transport theorem to combine the $\nabla \cdot \mathbf{w}_+$ term in (1.6) with the material derivative and rewrite them into a derivative structure,

$$(\partial_t^* \mathbf{u}_+(t), \mathbf{v}_+(t))_{\Omega_+(t)} + \frac{1}{2} (\mathbf{u}_+(t), \mathbf{v}_+(t) \nabla \cdot \mathbf{w}_+(t))_{\Omega_+(t)}$$

$$= \frac{1}{2} \frac{d}{dt} (\mathbf{u}_+(t), \mathbf{v}_+(t))_{\Omega_+(t)} + \frac{1}{2} (\partial_t^\bullet \mathbf{u}_+(t), \mathbf{v}_+(t))_{\Omega_+(t)}, \quad (1.8)$$

where ∂_t^\bullet is the material derivative with respect to \mathbf{w}_+ (see (2.1)) and $\mathbf{v}_+(t)$ is the test function which automatically satisfies the vanishing material derivative property. Let τ denote the time step size, Ω_+^n the approximate domain at t_n , $\phi^n : \Omega_+^n \rightarrow \Omega_+^{n+1}$ the approximate flow map. Let \mathbf{v}_+ denote a test function on Ω_+^{n+1} . Applying the Euler method to discretize (1.8) at $t = t_n$ as follows,

$$\frac{d}{dt} \Big|_{t=t_n} (\mathbf{u}_+(t), \mathbf{v}_+)_{\Omega_+(t)} \approx \frac{1}{\tau} ((\mathbf{u}_+^{n+1}, \mathbf{v}_+)_{\Omega_+^{n+1}} - (\mathbf{u}_+^n, \mathbf{v}_+ \circ \phi^n)_{\Omega_+^n}), \quad (1.9)$$

$$(\partial_t^\bullet \mathbf{u}_+(t_n), \mathbf{v}_+)_{\Omega_+(t_n)} \approx \frac{1}{\tau} (\mathbf{u}_+^{n+1} \circ \phi^n - \mathbf{u}_+^n, \mathbf{v}_+ \circ \phi^n)_{\Omega_+^n}, \quad (1.10)$$

we derive the following discretization of (1.8) which can be proved to be energy-dissipating at the discrete time level:

$$\frac{1}{2\tau} [(\mathbf{u}_+^{n+1}, \mathbf{v}_+)_{\Omega_+^{n+1}} - (\mathbf{u}_+^n, \mathbf{v}_+ \circ \phi^n)_{\Omega_+^n}] + \frac{1}{2\tau} (\mathbf{u}_+^{n+1} \circ \phi^n - \mathbf{u}_+^n, \mathbf{v}_+ \circ \phi^n)_{\Omega_+^n}.$$

The energy-dissipating property of the proposed scheme plays an essential role in the unique solvability of the velocity part as well as the long time simulation in practical computation. Moreover, inspired by [13], we prove the inf-sup conditions for Taylor-Hood elements on non-matching meshes. This guarantees the unique solvability of the whole system and ensures the robustness of the proposed approach.

The rest of this paper is organized as follows. After briefly introducing the sliding interface method, we state the main results of this paper, including the derivation of the fully discrete scheme and the main theorems addressing the unique solvability and energy-dissipating property of the proposed scheme in Section 2. In Section 3, we prove the main theorems by establishing an inf-sup stability result of the composite Taylor-Hood pairs on the non-matching isoparametric meshes. In Section 4, several numerical experiments are performed to validate the efficiency of the proposed numerical method. Finally, some conclusions are drawn in Section 5.

2. The numerical method and main results. In this section, we first introduce the sliding interface method, in which the subproblem on the rotating subdomain is rewritten in the ALE formulation and coupled with the subproblem on the stationary domain by the Nitsche's method. After the derivation of the equivalent formulation of the continuous problem, we present the fully discrete scheme and the main theorem.

2.1. The sliding interface method and the ALE formulation of subproblems.

We focus on only the fluid part and introduce the sliding interface method. For simplicity, and without loss of generality, we set $\rho_f = 1$ and assume that $\Gamma_+(t)$ lies inside the unit circle. For the FSI problem with a rigid structure, $\Gamma_+(t)$ is purely rotating around the z axis. In this case the position of $\Gamma_+(t)$ is described by its rotating angle $\theta(t)$, or the rotating matrix $R(\theta(t))$. We have

$$R(\theta) = \begin{pmatrix} \cos \theta & -\sin \theta & 0 \\ \sin \theta & \cos \theta & 0 \\ 0 & 0 & 1 \end{pmatrix}, \quad d = 3; \quad R(\theta) = \begin{pmatrix} \cos \theta & -\sin \theta \\ \sin \theta & \cos \theta \end{pmatrix}, \quad d = 2.$$

The anticlockwise rotating velocity field \mathbf{v}^R with the unit speed writes

$$\mathbf{v}^R = (-y, x, 0)^T, \quad d = 3, \quad \mathbf{v}^R = (-y, x)^T, \quad d = 2,$$

and $\mathbf{v}_{\Gamma_+} = \mathbf{v}^R|_{\Gamma_+}$. In order to deal with the rotational interior boundary, we introduce a sliding interface to enclose it. We consider Γ , the unit circle, which divides the entire domain into two subdomains, i.e. the rotating fluid domain $\Omega_+(t)$ and the stationary fluid domain Ω_- ,

$$\Gamma = \overline{\Omega_+(t)} \cap \overline{\Omega_-} \quad \text{and} \quad \Omega = \Omega_+(t) \cup \Omega_- \cup \Gamma,$$

see Fig 1.1b. We should emphasize that the symmetric property of the sliding interface Γ yields $\Omega_+(t) = R(\theta(t))\Omega_+(0)$. This property implies that $\Omega_+(t)$ can be isometrically mapped back to $\Omega_+(0)$, which guarantees the effectiveness of applying the ALE method for subproblem on $\Omega_+(t)$.

To describe the subproblems in both the moving and fixed subdomains in a uniform way, we also view the fixed subdomain Ω_- as a moving one, denoted by $\Omega_-(t)$, with a vanishing velocity. We consider the flow maps of these subdomains: $\Phi_{\pm}(t) : \Omega_{\pm}(0) \rightarrow \Omega_{\pm}(t)$, where $\Phi_-(t)$ is the identity map. The ALE moving frame associated to this mapping has velocity $\mathbf{w}_{\pm} = \partial_t \Phi_{\pm} \circ \Phi_{\pm}^{-1}$. The associated material derivatives are

$$\partial_t^{\bullet} \mathbf{u}_{\pm} := \partial_t \mathbf{u}_{\pm} + \mathbf{w}_{\pm} \cdot \nabla \mathbf{u}_{\pm}. \quad (2.1)$$

Let us recall the transport theorem [32, Lemma 5.7] governing the evolution of integrals over time-dependent domains. For any sufficiently regular function $g : \bigcup_{t \in [0, T]} (\Omega_+(t) \times \{t\}) \rightarrow \mathbb{R}$, the following holds:

$$\frac{d}{dt} \int_{\Omega_+(t)} g(x, t) dx = \int_{\Omega_+(t)} (\partial_t^{\bullet} g + g \nabla \cdot \mathbf{w}_+) dx. \quad (2.2)$$

Since Ω_- is stationary, $\mathbf{w}_- = 0$ and the associated material derivative is the standard Eulerian derivative.

We now discuss the selection of the ALE velocity field \mathbf{w}_+ . For FSI problems involving a rotating rigid body, the domain $\Omega_+(t)$ evolves according to $\Omega_+(t) = R(\theta(t))\Omega_+(0)$. In this case, the most natural choice for \mathbf{w}_+ is the rotational velocity field:

$$\mathbf{w}_+(t) = \omega(t) \mathbf{v}^R. \quad (2.3)$$

This rotational velocity field corresponds to a special case of the general ALE velocity obtained via harmonic extension, where $\mathbf{w}_{\Gamma}(t) = \omega(t) \mathbf{v}^R|_{\Gamma}$, and $\mathbf{w}_D(t) = \omega(t) \mathbf{v}_{\Gamma_+}$:

$$\Delta \mathbf{w}_+(t) = \mathbf{0}, \quad \text{in } \Omega_+(t), \quad (2.4)$$

$$\mathbf{w}_+(t) = \mathbf{w}_{\Gamma}(t), \quad \text{on } \Gamma, \quad (2.5)$$

$$\mathbf{w}_+(t) = \mathbf{w}_D(t), \quad \text{on } \Gamma_+(t). \quad (2.6)$$

In general, \mathbf{w}_{Γ} only needs to be a tangential vector field on Γ . Thus, the harmonic extension in (2.4)–(2.6) provides more flexibility than the purely rotational case (2.3). However, this flexibility comes at a cost: the resulting \mathbf{w}_+ is no longer divergence-free. Furthermore, such harmonic extensions may be unavoidable for Dirichlet problems where the interior motion \mathbf{w}_D is prescribed and not purely rotational. For these reasons, the divergence-free condition on \mathbf{w}_+ is not enforced in the subsequent analysis.

The Navier-Stokes equations on moving domains (1.1a)–(1.1b) with Dirichlet boundary conditions can be reformulated in the ALE framework as a coupled system of two subproblems. Consider the solutions (\mathbf{u}_+, p_+) and (\mathbf{u}_-, p_-) satisfying the following equations:

$$\partial_t^{\bullet} \mathbf{u}_{\pm} + (\mathbf{u}_{\pm} - \mathbf{w}_{\pm}) \cdot \nabla \mathbf{u}_{\pm} - \nabla \cdot \boldsymbol{\sigma}(\mathbf{u}_{\pm}, p_{\pm}) = \mathbf{f} \quad \text{in } \bigcup_{t \in (0, T]} \Omega_{\pm}(t) \times \{t\}, \quad (2.7a)$$

$$\nabla \cdot \mathbf{u}_{\pm} = 0 \quad \text{in } \bigcup_{t \in (0, T]} \Omega_{\pm}(t) \times \{t\}, \quad (2.7b)$$

with Dirichlet boundary conditions:

$$\mathbf{u}_- = \mathbf{0} \quad \text{on } \bigcup_{t \in [0, T]} \Gamma_- \times \{t\}, \quad (2.7c)$$

$$\mathbf{u}_+ = \mathbf{w}_D(t) \quad \text{on } \bigcup_{t \in [0, T]} \Gamma_+(t) \times \{t\}, \quad (2.7d)$$

and coupling conditions at the interface:

$$\mathbf{u}_+ = \mathbf{u}_- \quad \text{on } \bigcup_{t \in (0, T]} \Gamma \times \{t\}, \quad (2.7e)$$

$$\boldsymbol{\sigma}(\mathbf{u}_+, p_+) \mathbf{n} = \boldsymbol{\sigma}(\mathbf{u}_-, p_-) \mathbf{n} \quad \text{on } \bigcup_{t \in (0, T]} \Gamma \times \{t\}. \quad (2.7f)$$

For the FSI problem (1.1), one replaces the Dirichlet boundary conditions (2.7c)–(2.7d) by

$$\mathbf{u}_- = 0 \quad \text{on } \Gamma_-, \quad (2.7g)$$

$$\mathbf{u}_+ = \omega(t) \mathbf{v}_{\Gamma_+(t)} \quad \text{on } \bigcup_{t \in (0, T]} \Gamma_+(t) \times \{t\}, \quad (2.7h)$$

and includes the structural dynamics equation from (1.1e):

$$I_s \omega'(t) = \int_{\Gamma_+(t)} (\boldsymbol{\sigma}(\mathbf{u}_+, p_+) \cdot \mathbf{n}_s) \cdot \mathbf{v}_{\Gamma_+}. \quad (2.7i)$$

The coupled system (2.7a)–(2.7b) and (2.7e)–(2.7i) constitutes the equivalent ALE sliding interface formulation of the rotating rigid-body FSI problem (1.1).

2.2. Weak formulation of the Dirichlet problem. In this section, we derive the weak formulation of the Dirichlet problem (2.7a)–(2.7f). Let us define spaces

$$\mathbf{V}_+^D = \{\mathbf{v} \in [H^1(\Omega_+(t))]^d : \mathbf{v} = \mathbf{w}_D(t) \text{ on } \Gamma_+(t)\},$$

$$\mathbf{V}_\pm = \{\mathbf{v} \in [H^1(\Omega_\pm(t))]^d : \mathbf{v} = 0 \text{ on } \Gamma_\pm(t)\}, \quad Q_\pm(t) = L^2(\Omega_\pm(t)),$$

$$\dot{Q}(t) = \{(q_+, q_-) \in L^2(\Omega_+(t)) \times L^2(\Omega_-) : \int_{\Omega_+(t)} q_+ \, dx + \int_{\Omega_-} q_- \, dx = 0\}.$$

We use $(\cdot, \cdot)_{\Omega_\pm}$ to denote the L^2 inner product on the domain Ω_\pm , and $\langle \cdot, \cdot \rangle_\Gamma$ denotes the L^2 inner product on the sliding interface Γ .

To derive the weak formulation of (2.7a)–(2.7f), we test $\mathbf{v} = (\mathbf{v}_+, \mathbf{v}_-) \in \mathbf{V}_+ \times \mathbf{V}_-$ on (2.7a) and $(q_+, q_-) \in \dot{Q}(t)$ on (2.7b). According to (1.6), we can reformulate the convection term into a skew-symmetric form with some boundary terms. According to the choice of \mathbf{w}_+ in (2.3) or (2.4)–(2.6), since \mathbf{w}_Γ is tangential to Γ , we obtain $\mathbf{w}_+ \cdot \mathbf{n} = 0$ on Γ . Furthermore, making use of the following facts: \mathbf{u}_\pm satisfies the incompressible conditions and $\mathbf{u}_i - \mathbf{w}_i = 0$ on $\Gamma_i(t)$ for $i = \pm$, we obtain

$$\begin{aligned} \sum_{i=\pm} ((\mathbf{u}_i - \mathbf{w}_i) \cdot \nabla \mathbf{u}_i, \mathbf{v}_i)_{\Omega_i} &= \sum_{i=\pm} b_i (\mathbf{u}_i - \mathbf{w}_i; \mathbf{u}_i, \mathbf{v}_i) + \sum_{i=\pm} \frac{1}{2} (\mathbf{u}_i, \mathbf{v}_i \nabla \cdot \mathbf{w}_i)_{\Omega_i} \\ &\quad + \frac{1}{2} \int_\Gamma (\mathbf{u}_+ \cdot \mathbf{n}) \mathbf{u}_+ \cdot \mathbf{v}_+ - (\mathbf{u}_- \cdot \mathbf{n}) \mathbf{u}_- \cdot \mathbf{v}_- \, dA, \end{aligned}$$

where \mathbf{n} denotes the normal vector of Γ from $\Omega_+(t)$ to Ω_- . Now we apply the coupling condition (2.7e) on Γ , which indicates that the average defined below is equal to both $(\mathbf{u}_\pm \cdot \mathbf{n}) \mathbf{u}_\pm$ on Γ ,

$$\langle \{(\mathbf{u} \cdot \mathbf{n}) \mathbf{u}\} \rangle := \frac{1}{2} ((\mathbf{u}_+ \cdot \mathbf{n}) \mathbf{u}_+ + (\mathbf{u}_- \cdot \mathbf{n}) \mathbf{u}_-) \Big|_\Gamma.$$

Thus, we obtain

$$\begin{aligned} \sum_{i=\pm} ((\mathbf{u}_i - \mathbf{w}_i) \cdot \nabla \mathbf{u}_i, \mathbf{v}_i)_{\Omega_i} &= \sum_{i=\pm} [b_i (\mathbf{u}_i - \mathbf{w}_i; \mathbf{u}_i, \mathbf{v}_i) + \frac{1}{2} (\mathbf{u}_i, \mathbf{v}_i \nabla \cdot \mathbf{w}_i)_{\Omega_i}] \\ &\quad + \frac{1}{2} \langle \{(\mathbf{u} \cdot \mathbf{n}) \mathbf{u}\} \rangle, \llbracket \mathbf{v} \rrbracket \Big|_\Gamma, \end{aligned} \quad (2.8)$$

where $\llbracket \mathbf{v} \rrbracket = (\mathbf{v}_+ - \mathbf{v}_-) \Big|_\Gamma$. Similar treatment can be applied to $(\nabla \cdot \boldsymbol{\sigma}(\mathbf{u}_\pm, p_\pm), \mathbf{v}_\pm)_{\Omega_i}$ by applying the integration by parts and (2.7f). This yields

$$\begin{aligned} - \sum_{i=\pm} (\nabla \cdot \boldsymbol{\sigma}(\mathbf{u}_i, p_i), \mathbf{v}_i)_{\Omega_i} &= \sum_{i=\pm} (2\mu \mathbb{D} \mathbf{u}_i, \mathbb{D} \mathbf{v}_i)_{\Omega_i} - \sum_{i=\pm} (p_i, \nabla \cdot \mathbf{v}_i)_{\Omega_i} \\ &\quad - \langle \{(\boldsymbol{\sigma}(\mathbf{u}, p) \mathbf{n})\} \rangle, \llbracket \mathbf{v} \rrbracket \Big|_\Gamma. \end{aligned} \quad (2.9)$$

Adding these results together, we obtain

$$\begin{aligned} & \sum_{i=\pm} \left[(\partial_t^\bullet \mathbf{u}_i, \mathbf{v}_i)_{\Omega_i} + b_i(\mathbf{u}_i - \mathbf{w}_i; \mathbf{u}_i, \mathbf{v}_i) + \frac{1}{2}(\mathbf{u}_i, \mathbf{v}_i \nabla \cdot \mathbf{w}_i)_{\Omega_i} \right] \\ & \quad + \sum_{i=\pm} \left[(2\mu \mathbb{D} \mathbf{u}_i, \mathbb{D} \mathbf{v}_i)_{\Omega_i} + (q_i, \nabla \cdot \mathbf{u}_i)_{\Omega_i} - (p_i, \nabla \cdot \mathbf{v}_i)_{\Omega_i} \right] \\ & \quad + \frac{1}{2} \langle \{ \{ (\mathbf{u} \cdot \mathbf{n}) \mathbf{u} \} \}, [\mathbf{v}] \rangle_\Gamma - \langle \{ \{ \boldsymbol{\sigma}(\mathbf{u}, p) \mathbf{n} \} \}, [\mathbf{v}] \rangle_\Gamma = \sum_{i=\pm} (\mathbf{f}, \mathbf{v}_i)_{\Omega_i}. \end{aligned}$$

Taking account for the continuity conditions of \mathbf{u} results in the following equivalent formulation for the smooth solution case:

$$\begin{aligned} & \sum_{i=\pm} \left[(\partial_t^\bullet \mathbf{u}_i, \mathbf{v}_i)_{\Omega_i} + b_i(\mathbf{u}_i - \mathbf{w}_i; \mathbf{u}_i, \mathbf{v}_i) + \frac{1}{2}(\mathbf{u}_i, \mathbf{v}_i \nabla \cdot \mathbf{w}_i)_{\Omega_i} + (2\mu \mathbb{D} \mathbf{u}_i, \mathbb{D} \mathbf{v}_i)_{\Omega_i} \right] \\ & \quad + \frac{1}{2} \langle \{ \{ (\mathbf{u} \cdot \mathbf{n}) \mathbf{u} \} \}, [\mathbf{v}] \rangle_\Gamma - \langle \{ \{ \boldsymbol{\sigma}(\mathbf{u}, p) \mathbf{n} \} \}, [\mathbf{v}] \rangle_\Gamma + \sum_{i=\pm} \left[(q_i, \nabla \cdot \mathbf{u}_i)_{\Omega_i} - (p_i, \nabla \cdot \mathbf{v}_i)_{\Omega_i} \right] \\ & \quad - \frac{1}{2} \langle \{ \{ (\mathbf{u} \cdot \mathbf{n}) \mathbf{v} \} \}, [\mathbf{u}] \rangle_\Gamma + \langle \{ \{ \boldsymbol{\sigma}(\mathbf{v}, q) \mathbf{n} \} \}, [\mathbf{u}] \rangle_\Gamma = \sum_{i=\pm} (\mathbf{f}, \mathbf{v}_i)_{\Omega_i}. \end{aligned}$$

For clarity, we introduce the following notations

$$\begin{aligned} A(\mathbf{z}; \mathbf{u}, \mathbf{v}) & := \sum_{i=\pm} (2\mu \mathbb{D} \mathbf{u}_i, \mathbb{D} \mathbf{v}_i)_{\Omega_i} + \frac{1}{2} \langle \{ \{ (\mathbf{z} \cdot \mathbf{n}) \mathbf{u} \} \}, [\mathbf{v}] \rangle_\Gamma - \frac{1}{2} \langle \{ \{ (\mathbf{z} \cdot \mathbf{n}) \mathbf{v} \} \}, [\mathbf{u}] \rangle_\Gamma \\ & \quad - 2\mu \langle \{ \{ \mathbb{D}(\mathbf{u}) \mathbf{n} \} \}, [\mathbf{v}] \rangle_\Gamma + 2\mu \langle \{ \{ \mathbb{D}(\mathbf{v}) \mathbf{n} \} \}, [\mathbf{u}] \rangle_\Gamma, \end{aligned} \quad (2.10)$$

$$B(\mathbf{u}, q) := \sum_{i=\pm} -(q_i, \nabla \cdot \mathbf{u}_i)_{\Omega_i} + \langle \{ \{ q \mathbf{n} \} \}, [\mathbf{u}] \rangle_\Gamma, \quad (2.11)$$

where $\{ \{ \mathbb{D}(\mathbf{v}) \mathbf{n} \} \} = \frac{1}{2}(\mathbb{D}(\mathbf{v}_+) \mathbf{n} + \mathbb{D}(\mathbf{v}_-) \mathbf{n})$ denotes the average of $\mathbb{D}(\mathbf{v}_\pm) \mathbf{n}$ on the interface. Then, the weak formulation is to seek $(\mathbf{u}_+, \mathbf{u}_-, p_+, p_-) \in L^\infty(0, T; \mathbf{V}_+^D \times \mathbf{V}_- \times \dot{Q})$ such that

$$\begin{aligned} & \sum_{i=\pm} \left[(\partial_t^\bullet \mathbf{u}_i, \mathbf{v}_i)_{\Omega_i} + b_i(\mathbf{u}_i - \mathbf{w}_i; \mathbf{u}_i, \mathbf{v}_i) + \frac{1}{2}(\mathbf{u}_i, \mathbf{v}_i \nabla \cdot \mathbf{w}_i)_{\Omega_i} \right] \\ & \quad + A(\mathbf{u}; \mathbf{u}, \mathbf{v}) + B(\mathbf{v}, p) - B(\mathbf{u}, q) = \sum_{i=\pm} (\mathbf{f}, \mathbf{v}_i)_{\Omega_i}, \end{aligned} \quad (2.12)$$

holds for $(\mathbf{v}_+, \mathbf{v}_-, q_+, q_-) \in L^\infty(0, T; \mathbf{V}_+ \times \mathbf{V}_- \times \dot{Q})$. The uniqueness of solutions to (2.12) follows from standard energy estimates.

2.3. Weak formulation of FSI and energy-dissipation property. For the derivation of the weak formulation for the FSI problem with a rigid rotating structure, we need to pay special attention to the coupling condition (2.7h) on $\Gamma_+(t)$. Since the rotating speed $\omega(t)$ is an unknown, the spaces for the solution and test functions have an additional degree of freedom. The trial and test function spaces are changed to be

$$\mathbf{V}^f = (\mathbf{V}_+ \times \mathbf{V}_-) \oplus \text{span}\{(\mathbf{v}^R, 0)\}. \quad (2.13)$$

We shall emphasize that for test function $(\mathbf{v}_+, \mathbf{v}_-) \in \mathbf{V}^f$, \mathbf{v}_+ may not vanish on $\Gamma_+(t)$. It has no effect on the derivation of (2.8), but (2.9) needs to be modified. For $(\mathbf{v}_+, \mathbf{v}_-) \in \mathbf{V}^f$, satisfying $\mathbf{v}_+|_{\Gamma_+(t)} = \lambda \mathbf{v}_{\Gamma_+(t)}$, we have

$$\begin{aligned} - \sum_{i=\pm} (\nabla \cdot \boldsymbol{\sigma}(\mathbf{u}_i, p_i), \mathbf{v}_i)_{\Omega_i} & = \sum_{i=\pm} (2\mu \mathbb{D} \mathbf{u}_i, \mathbb{D} \mathbf{v}_i)_{\Omega_i} - \sum_{i=\pm} (p_i, \nabla \cdot \mathbf{v}_i)_{\Omega_i} \\ & \quad - \langle \{ \{ \boldsymbol{\sigma}(\mathbf{u}, p) \mathbf{n} \} \}, [\mathbf{v}] \rangle_\Gamma + \lambda \int_{\Gamma_+} (\boldsymbol{\sigma}(\mathbf{u}, p) \cdot \mathbf{n}_s) \cdot \mathbf{v}_{\Gamma_+}, \end{aligned}$$

where \mathbf{n}_s denotes the normal vector of Γ_+ pointing from Ω_s to Ω .

Let $\theta(t) = \int_0^t \omega(s) ds$ denote the unknown rotating angle. $\Omega_+(t)$ is mapped from $\Omega_+(0)$ by $R(\theta(t))$, and the function spaces on $\Omega_+(t)$ are also pushed forward from those on $\Omega_+(0)$. Using (1.1e), the weak formulation is to seek $\omega(t) \in C^1([0, T]; \mathbb{R})$ and $(\mathbf{u}_+, \mathbf{u}_-, p_+, p_-) \in L^\infty(0, T; \mathbf{V}^f(t) \times \dot{Q}(t))$ such that $\mathbf{u}_+(t)|_{\Gamma_+(t)} = \omega(t)\mathbf{v}_{\Gamma_+(t)}$ and

$$\begin{aligned} \sum_{i=\pm} \left[(\partial_t^\bullet \mathbf{u}_i, \mathbf{v}_i)_{\Omega_i} + b_i(\mathbf{u}_i - \mathbf{w}_i; \mathbf{u}_i, \mathbf{v}_i) + \frac{1}{2}(\mathbf{u}_i, \mathbf{v}_i \nabla \cdot \mathbf{w}_i)_{\Omega_i} \right] + A(\mathbf{u}; \mathbf{u}, \mathbf{v}) \\ + B(\mathbf{v}, p) - B(\mathbf{u}, q) + \lambda I_s \omega'(t) = \sum_{i=\pm} (\mathbf{f}, \mathbf{v}_i)_{\Omega_i}, \end{aligned} \quad (2.14)$$

hold for any $(\mathbf{v}_+, \mathbf{v}_-, q_+, q_-, \lambda) \in L^\infty(0, T; \mathbf{V}^f(t) \times \dot{Q}(t) \times \mathbb{R})$ which satisfies $\mathbf{v}_+|_{\Gamma_+(t)} = \lambda \mathbf{v}_{\Gamma_+(t)}$. The total energy of the FSI problem is defined by

$$E(t) = \frac{1}{2} \sum_{i=\pm} \int_{\Omega_i} |\mathbf{u}_i|^2 dx + \frac{1}{2} I_s \omega^2. \quad (2.15)$$

When there is no external force \mathbf{f} , the total energy of the FSI system dissipates.

Lemma 2.1. *Assume $\mathbf{f} = 0$. Let $\omega(t)$ and $(\mathbf{u}_+, \mathbf{u}_-, p_+, p_-)$ be a smooth solution of weak formulation (2.14). Then, $(\mathbf{u}_+, \mathbf{u}_-)$ satisfies the energy dissipation law*

$$\frac{d}{dt} E(t) = -2\mu(\|\mathbb{D}(\mathbf{u}_+)\|^2 + \|\mathbb{D}(\mathbf{u}_-)\|^2) \leq 0.$$

Proof. Choosing $(\mathbf{v}_+, \mathbf{v}_-, q_+, q_-, \lambda) = (\mathbf{u}_+, \mathbf{u}_-, p_+, p_-, \omega)$ in (2.14) and using the skew-symmetric of $b_i(\mathbf{u}_i - \mathbf{w}_i; \cdot, \cdot)$, we get

$$\begin{aligned} (\partial_t^\bullet \mathbf{u}_+, \mathbf{u}_+)_{\Omega_+(t)} + \frac{1}{2}(\mathbf{u}_+, \mathbf{u}_+ \nabla \cdot \mathbf{w}_+)_{\Omega_+(t)} \\ + (\partial_t \mathbf{u}_-, \mathbf{u}_-)_{\Omega_-} + \sum_{i=\pm} (2\mu \mathbb{D} \mathbf{u}_i, \mathbb{D} \mathbf{u}_i)_{\Omega_i} + I_s \omega \omega' = 0. \end{aligned} \quad (2.16)$$

Next we apply the transport theorem (2.2) on $\Omega_+(t)$ and obtain

$$\frac{d}{dt} \int_{\Omega_+(t)} \frac{1}{2} |\mathbf{u}_+|^2 dx = (\partial_t^\bullet \mathbf{u}_+, \mathbf{u}_+)_{\Omega_+(t)} + \frac{1}{2}(\mathbf{u}_+, \mathbf{u}_+ \nabla \cdot \mathbf{w}_+)_{\Omega_+(t)}.$$

Thus, we obtain

$$\frac{d}{dt} \left[\sum_{i=\pm} \int_{\Omega_i} \frac{1}{2} |\mathbf{u}_i|^2 dx + \frac{1}{2} I_s \omega^2 \right] = - \sum_{i=\pm} (2\mu \mathbb{D} \mathbf{u}_i, \mathbb{D} \mathbf{u}_i)_{\Omega_i}. \quad (2.17)$$

This completes the proof of Lemma 2.1. \square

2.4. Isoparametric finite elements. Let $\{t_n\}_{n=0}^M$ be a uniform partition of $[0, T]$ with time step size $\tau = T/M$. For the initial subdomains $\Omega_i(0)$, let $\tilde{\mathcal{T}}_{hi}^0$ be the corresponding quasi-uniform and shape-regular triangulations and let $\tilde{\Omega}_{h\pm}^0 := \cup_{K \in \tilde{\mathcal{T}}_{h\pm}^0} K$ be the approximate subdomains. Since curved boundaries Γ and Γ_+ are involved, the boundary elements need to be modified into curved elements. Let \hat{K} denote the reference simplex. Each curved boundary simplex K is parametrized by a unique polynomial of degree m denoted by $F_K^m : \hat{K} \rightarrow K$. For details on its construction, we refer the interested readers to [24]. We denote the triangulation with these curved boundary elements as $\mathcal{T}_{h\pm}^0$. The finite element space of degree k on $\Omega_{h\pm}^0$ is defined as

$$V_{h\pm}^k := \left\{ g_h \in C(\Omega_{h\pm}^0) : g_h \circ F_K^m \in P^k(\hat{K}) \text{ for all } K \in \mathcal{T}_{h\pm}^0 \right\}.$$

In general, only the case $m = k$ is termed as the isoparametric FEM. However, later in this paper, the Taylor-Hood FEM will be used and the FEM spaces for the velocity and the pressure have different degree k and $k-1$, $k \geq 2$. We will choose $m = k-1$ and call it as the isoparametric Taylor-Hood element. In particular, for $k = 2$, it will become the standard Taylor-Hood element (P2-P1) on triangulation with straight edges. Compared with the isogeometric analysis approach [9], which eliminates geometric errors by representing the

geometry exactly, the isoparametric FEM introduces geometric approximation errors and non-matching meshes at artificial interfaces. Nevertheless, the isoparametric framework can allow us to rigorously prove the discrete inf-sup condition (Theorem 3.1), ensuring the well-posedness and stability of the fully discrete scheme. Additionally, it benefits from easier implementation due to its compatibility with widely available FEM software.

Let us denote $\Omega_{h\pm}^n := \cup_{K \in \mathcal{T}_{h\pm}^n} K$. Then Ω_{h-}^n is fixed and has two boundaries, Γ_{h-}^A and Γ_{h-} , which approximate Γ and Γ_- respectively. For the interior subdomain, the approximate interior subdomain Ω_{h+}^n at $t = t_n$ is described as the image of the discrete flow map $\Phi_{h+}^n : \Omega_{h+}^0 \rightarrow \Omega_{h+}^n$. For consistency, we introduce the notation of discrete flow map $\Phi_{h-}^n : \Omega_{h-}^0 \rightarrow \Omega_{h-}^n$, which is an identity map. Let us denote the boundaries of Ω_{h+}^n as $\Gamma_{h+}^{A,n}$ and Γ_{h+}^n , which approximate Γ and Γ_+ respectively.

On each subdomain Ω_{hi}^n with $i = \pm$, we introduce the following Taylor-Hood type finite element spaces,

$$\begin{aligned} \mathbf{V}_k(\Omega_{hi}^n) &= \{\mathbf{v}_h : \mathbf{v}_h \circ \Phi_{hi}^n \in [V_{hi}^k]^d\}, \\ \dot{\mathbf{V}}_k(\Omega_{hi}^n) &= \{\mathbf{v}_h \in \mathbf{V}_k(\Omega_{hi}^n) : \mathbf{v}|_{\partial\Omega_{hi}^n} = 0\}, \end{aligned} \quad (2.18)$$

$$\tilde{Q}_{k-1}(\Omega_{hi}^n) = \{q_h : q_h \circ \Phi_{hi}^n \in V_{hi}^{k-1}\}, \quad (2.19)$$

$$Q_{k-1}(\Omega_{hi}^n) = \{q_h : q_h \circ \Phi_{hi}^n \in V_{hi}^{k-1}, \int_{\Omega_{hi}^n} q_h dx = 0\}. \quad (2.20)$$

The following inf-sup condition is satisfied on each subdomain for the isoparametric Taylor-Hood elements, which can be proved by combining the Verfürth trick (see [11, Sect. 8.5]) and the perturbation argument in [14],

$$\|q_{hi}\|_{L^2(\Omega_{hi}^n)} \lesssim \sup_{0 \neq \mathbf{v}_{hi} \in \dot{\mathbf{V}}_k(\Omega_{hi}^n)} \frac{(\nabla \cdot \mathbf{v}_{hi}, q_{hi})_{\Omega_{hi}^n}}{\|\mathbf{v}_{hi}\|_{H^1(\Omega_{hi}^n)}}, \quad \forall q_{hi} \in Q_{k-1}(\Omega_{hi}^n). \quad (2.21)$$

We introduce the notation of local flow map $\phi_{h+}^n \in \mathbf{V}_m(\Omega_{hi}^n)$ that maps Ω_{h+}^n to Ω_{h+}^{n+1} :

$$\phi_{h+}^n := \Phi_{h+}^{n+1} \circ (\Phi_{h+}^n)^{-1} = \text{id} + \tau \mathbf{w}_{h+}^n, \quad (2.22)$$

where the mesh velocity $\mathbf{w}_{h+}^n \in \mathbf{V}_m(\Omega_{h+}^n)$ is either the interpolation of (2.3) or solved from the spatial discretization of (2.4)–(2.6): solving $\mathbf{w}_{h+}^n \in \mathbf{V}_m(\Omega_{h+}^n)$ such that for all test functions $\mathbf{v}_h \in \mathbf{V}_m(\Omega_{h+}^n)$ that

$$(\nabla \mathbf{w}_{h+}^n, \nabla \mathbf{v}_h)_{\Omega_{h+}^n} = 0, \quad (2.23)$$

$$\mathbf{w}_{h+}^n = I_{h+}^m \mathbf{w}_\Gamma, \quad \text{on } \Gamma_{h+}^{A,n}, \quad (2.24)$$

$$\mathbf{w}_{h+}^n = I_{h+}^m \mathbf{w}_D, \quad \text{on } \Gamma_{h+}^n, \quad (2.25)$$

where I_{h+}^m denotes the interpolation with respect to $\mathbf{V}_m(\Omega_{h+}^n)$.

Next, we construct the composite finite element spaces by combining the finite element spaces defined on each subdomain. We denote these spaces in curly characters.

$$\begin{aligned} \mathcal{V}_k^n &= \mathbf{V}_k(\Omega_{h+}^n) \times \mathbf{V}_k(\Omega_{h-}^n), \\ \dot{\mathcal{V}}_k^n &= \{(\mathbf{v}_{h+}, \mathbf{v}_{h-}) \in \mathcal{V}_k^n : \mathbf{v}_{h+}|_{\Gamma_{h+}^n} = 0, \mathbf{v}_{h-}|_{\Gamma_{h-}^n} = 0\}, \end{aligned} \quad (2.26)$$

$$\mathcal{Q}_{k-1}^n = \{(q_{h+}, q_{h-}) \in \tilde{Q}_{k-1}(\Omega_{h+}^n) \times \tilde{Q}_{k-1}(\Omega_{h-}^n) : \sum_{i \in \pm} \int_{\Omega_{hi}^n} q_{hi} = 0\}, \quad (2.27)$$

and

$$\mathcal{V}_k^{n,D} = \{(\mathbf{v}_{h+}, \mathbf{v}_{h-}) \in \mathcal{V}_k^n, \mathbf{v}_{h+}|_{\Gamma_{h+}^n} = I_{h+}^k \mathbf{w}_D(t_n), \mathbf{v}_{h-}|_{\Gamma_{h-}^n} = 0\}.$$

Next we define the average and jump functions across Γ for $\mathbf{v}_h \in \mathcal{V}_k^n$ and $q_h \in \mathcal{Q}_{k-1}^n$. We should emphasize that the definitions of these functions are quite different from the method in [9], where no geometrical discrepancy is involved in [9] due to isogeometric analysis. In isoparametric FEM, the approximate boundaries $\Gamma_{h\pm}^{A,n}$ do not match Γ , requiring the

extension of finite element functions to Γ . We only need to extend $q_{hi} \in V_{hi}^k$ to Γ for any boundary element K that have a $d-1$ -dimensional simplex F on $\Gamma_{hi}^{A,n}$. Denoting the corresponding curved simplex on Γ as \tilde{F} , and the curved element as \tilde{K} , we directly extend q_{hi} from K to \tilde{K} with the same expression. The following remark gives a concrete example.

Remark 2.1. For FEMs of degree k which satisfies $k \geq m$, the extension of a linear function in K remains the same formula in \tilde{K} .

Then, for $\mathbf{v}_h \in \mathcal{V}_k^n$, we define

$$\llbracket \mathbf{v}_h \rrbracket := \mathbf{v}_{h+}|_{\Gamma} - \mathbf{v}_{h-}|_{\Gamma}, \quad \{\{\mathbf{v}_h\}\} := \frac{1}{2}(\mathbf{v}_{h+}|_{\Gamma} + \mathbf{v}_{h-}|_{\Gamma}).$$

Furthermore, we introduce the following (semi-)norms for $\mathbf{v}_h \in \mathcal{V}_k^n$ and $q_h \in \mathcal{Q}_{k-1}^n$:

$$\|q_h\|_{L^2} = \sum_{i=\pm} \|q_{hi}\|_{L^2(\Omega_{hi}^n)}, \quad |\mathbf{v}_h|_1 = \sum_{i=\pm} \|\nabla \mathbf{v}_{hi}\|_{L^2(\Omega_{hi}^n)} + h^{-1/2} \|\llbracket \mathbf{v}_h \rrbracket\|_{L^2(\Gamma)},$$

and the following bilinear forms,

$$\begin{aligned} A_h^n(\mathbf{z}; \mathbf{u}, \mathbf{v}) &:= (2\mu \mathbb{D}\mathbf{u}_i, \mathbb{D}\mathbf{v}_i)_{\Omega_{hi}^n} + \frac{1}{2} \langle \{(\mathbf{z} \cdot \mathbf{n})\mathbf{u}\}, \llbracket \mathbf{v} \rrbracket \rangle_{\Gamma} - \frac{1}{2} \langle \{(\mathbf{z} \cdot \mathbf{n})\mathbf{v}\}, \llbracket \mathbf{u} \rrbracket \rangle_{\Gamma} \\ &\quad - 2\mu \langle \{ \mathbb{D}(\mathbf{u})\mathbf{n} \}, \llbracket \mathbf{v} \rrbracket \rangle_{\Gamma} + 2\mu \langle \{ \mathbb{D}(\mathbf{v})\mathbf{n} \}, \llbracket \mathbf{u} \rrbracket \rangle_{\Gamma}, \end{aligned} \quad (2.28)$$

$$B_h^n(\mathbf{v}, q) := - \sum_{i=\pm} (\operatorname{div} \mathbf{v}_i, q_i)_{\Omega_{hi}^n} + \langle \{q\}, \llbracket \mathbf{v} \cdot \mathbf{n} \rrbracket \rangle_{\Gamma}, \quad (2.29)$$

and $b_{hi}^n(\mathbf{z}; \mathbf{u}, \mathbf{v})$ by replacing Ω_i in (1.7) with Ω_{hi}^n .

2.5. Fully discrete numerical scheme and main theoretic results. We begin with the derivation of the fully discrete scheme for (2.12). First, we consider the spatial semi-discretization of (2.12) by replacing \mathbf{w}_i , ∂_t^\bullet , and Ω_i in (2.12) with their discrete counterparts \mathbf{w}_{hi} , $D_{th} := \partial_t + \mathbf{w}_{hi} \cdot \nabla$, and Ω_{hi} :

$$\begin{aligned} &(D_{th} \mathbf{u}_{h+}, \boldsymbol{\psi}_{h+})_{\Omega_{h+}(t)} + \frac{1}{2} (\mathbf{u}_{h+}, \boldsymbol{\psi}_{h+} \nabla \cdot \mathbf{w}_{h+})_{\Omega_{h+}(t)} + (\partial_t \mathbf{u}_{h-}, \boldsymbol{\psi}_{h-})_{\Omega_{h-}} + B_h(\boldsymbol{\psi}_h, p_h) \\ &+ \sum_{i=\pm} b_{hi}(\mathbf{u}_{hi} - \mathbf{w}_{hi}; \mathbf{u}_{hi}, \boldsymbol{\psi}_{hi}) + A_h(\mathbf{u}_{hi}; \mathbf{u}_{hi}, \boldsymbol{\psi}_{hi}) - B_h(\mathbf{u}_h, q_h) = \sum_{i=\pm} (\mathbf{f}, \boldsymbol{\psi}_{hi})_{\Omega_{hi}}, \end{aligned} \quad (2.30)$$

where b_{hi} , A_h , and B_h denote the corresponding bilinear forms analogous to those defined in (1.7) and (2.10)–(2.11), but with the exact domain Ω_i replaced by its approximation Ω_{hi} .

Similar to the transport theorem (2.2), we also have the discrete version: for g_h defined on $\cup_{t \in [0, T]} \Omega_{h+}(t) \times \{t\}$:

$$\frac{d}{dt} \int_{\Omega_{h+}(t)} g_h(x, t) dx = \int_{\Omega_{h+}(t)} D_{th} g_h dx + \int_{\Omega_{h+}(t)} g_h(x, t) \nabla \cdot \mathbf{w}_{h+} dx.$$

Thus, for $\mathbf{u}_{h+}(x, t)$ and $\boldsymbol{\psi}_{h+}(x, t)$ defined on $\cup_{t \in [0, T]} \Omega_{h+}(t) \times \{t\}$, we have

$$\frac{d}{dt} (\mathbf{u}_{h+}, \boldsymbol{\psi}_{h+})_{\Omega_{h+}} = (D_{th} \mathbf{u}_{h+}, \boldsymbol{\psi}_{h+})_{\Omega_{h+}} + (\mathbf{u}_{h+}, D_{th} \boldsymbol{\psi}_{h+})_{\Omega_{h+}} + (\mathbf{u}_{h+}, \boldsymbol{\psi}_{h+} \nabla \cdot \mathbf{w}_{h+})_{\Omega_{h+}}.$$

Then the first two terms in (2.30) can be reformulated into:

$$\frac{1}{2} \frac{d}{dt} (\mathbf{u}_{h+}, \boldsymbol{\psi}_{h+})_{\Omega_{h+}(t)} - \frac{1}{2} (\mathbf{u}_{h+}, D_{th} \boldsymbol{\psi}_{h+})_{\Omega_{h+}(t)} + \frac{1}{2} (D_{th} \mathbf{u}_{h+}, \boldsymbol{\psi}_{h+})_{\Omega_{h+}(t)}. \quad (2.31)$$

Next, we discuss the temporal discretization of (2.31). Given a test function \mathbf{v}_{h+} defined on $\Omega_{h+}^{n+1} = \phi_{h+}^n(\Omega_{h+}^n)$, we choose the space-time test function such that $D_{th} \boldsymbol{\psi}_{h+} = 0$ and $\boldsymbol{\psi}_{h+}(t_{n+1}) = \mathbf{v}_{h+}$. Thus the second term in (2.31) vanishes and $\boldsymbol{\psi}_{h+}(t_n) = \mathbf{v}_{h+} \circ \phi_{h+}^n$. Thus, we discretize (2.31) as follows:

$$\begin{aligned} \frac{d}{dt} \Big|_{t=t_n} (\mathbf{u}_{h+}, \boldsymbol{\psi}_{h+})_{\Omega_{h+}(t)} &= \frac{1}{\tau} [(\mathbf{u}_{h+}^{n+1}, \mathbf{v}_{h+})_{\Omega_{h+}^{n+1}} - (\mathbf{u}_{h+}^n, \mathbf{v}_{h+} \circ \phi_{h+}^n)_{\Omega_{h+}^n}] + \mathcal{O}(\tau), \\ (D_{th} \mathbf{u}_{h+}, \boldsymbol{\psi}_{h+})_{\Omega_{h+}(t_n)} &= \frac{1}{\tau} (\mathbf{u}_{h+}^{n+1} \circ \phi_{h+}^n - \mathbf{u}_{h+}^n, \mathbf{v}_{h+} \circ \phi_{h+}^n)_{\Omega_{h+}^n} + \mathcal{O}(\tau), \end{aligned}$$

which leads to the following fully discrete scheme for (2.12):

Step 1: For given $\Omega_{h\pm}^n$ and $\mathbf{u}_{h\pm}^n$, solve \mathbf{w}_{h+}^n from (2.23)–(2.25). Set

$$\phi_{h+}^n = \text{id} + \tau \mathbf{w}_{h+}^n. \quad (2.32a)$$

Step 2: Let $\Omega_{h+}^{n+1} = \phi_{h+}^n(\Omega_{h+}^n)$. Find $(\mathbf{u}_h^{n+1}, p_h^{n+1}) \in \mathcal{V}_k^{n+1,D} \times \mathcal{Q}_{k-1}^{n+1}$ such that

$$\begin{aligned} & \frac{1}{2\tau} [(\mathbf{u}_{h+}^{n+1}, \mathbf{v}_{h+})_{\Omega_{h+}^{n+1}} - (\mathbf{u}_{h+}^n, \mathbf{v}_{h+} \circ \phi_{h+}^n)_{\Omega_{h+}^n}] + \frac{1}{2\tau} (\mathbf{u}_{h+}^{n+1} \circ \phi_{h+}^n - \mathbf{u}_{h+}^n, \mathbf{v}_{h+} \circ \phi_{h+}^n)_{\Omega_{h+}^n} \\ & + \frac{1}{\tau} (\mathbf{u}_{h-}^{n+1} - \mathbf{u}_{h-}^n, \mathbf{v}_{h-})_{\Omega_{h-}} + \sum_{i=\pm} b_{hi}^{n+1} ((\mathbf{u}_{hi}^n - \mathbf{w}_{hi}^n) \circ (\phi_{h+}^n)^{-1}; \mathbf{u}_{hi}^{n+1}, \mathbf{v}_{hi}) \\ & + A_h^{n+1}(\mathbf{u}_h^n \circ (\phi_{h+}^n)^{-1}; \mathbf{u}_h^{n+1}, \mathbf{v}_h) + B_h^{n+1}(\mathbf{v}_h, p_h^{n+1}) - B_h^{n+1}(\mathbf{u}_h^{n+1}, q_h) = \sum_{i=\pm} (\mathbf{f}^{n+1}, \mathbf{v}_{hi}), \end{aligned} \quad (2.32b)$$

holds for all $(\mathbf{v}_h, q_h) \in \dot{\mathcal{V}}_k^{n+1} \times \mathcal{Q}_{k-1}^{n+1}$.

Fully discrete scheme for (2.14) without external force, i.e., $\mathbf{f} = 0$:

Step 1: For given $\Omega_{h\pm}^n$, ω^n and $\mathbf{u}_{h\pm}^n$, determine \mathbf{w}_{h+}^n by interpolating (2.3) or solving from (2.23)–(2.25) with $\mathbf{w}_D = \omega^n \mathbf{v}_{\Gamma_+}$. Set

$$\phi_{h+}^n = \text{id} + \tau \mathbf{w}_{h+}^n. \quad (2.33a)$$

Step 2: Let $\Omega_{h+}^{n+1} = \phi_{h+}^n(\Omega_{h+}^n)$. Find $(\mathbf{u}_h^{n+1}, p_h^{n+1}, \omega^{n+1}) \in \mathcal{V}_k^{n+1} \times \mathcal{Q}_{k-1}^{n+1} \times \mathbb{R}$ such that

$$\mathbf{u}_h^{n+1}|_{\Gamma_{h+}^{n+1}} = \omega^{n+1} \mathbf{v}^R|_{\Gamma_{h+}^{n+1}}, \quad \mathbf{u}_h^{n+1}|_{\Gamma_{h-}^{n+1}} = 0, \quad (2.33b)$$

and

$$\begin{aligned} & \frac{1}{2\tau} [(\mathbf{u}_{h+}^{n+1}, \mathbf{v}_{h+})_{\Omega_{h+}^{n+1}} - (\mathbf{u}_{h+}^n, \mathbf{v}_{h+} \circ \phi_{h+}^n)_{\Omega_{h+}^n}] + \frac{1}{2\tau} (\mathbf{u}_{h+}^{n+1} \circ \phi_{h+}^n - \mathbf{u}_{h+}^n, \mathbf{v}_{h+} \circ \phi_{h+}^n)_{\Omega_{h+}^n} \\ & + \frac{1}{\tau} (\mathbf{u}_{h-}^{n+1} - \mathbf{u}_{h-}^n, \mathbf{v}_{h-})_{\Omega_{h-}} + \frac{1}{\tau} I_s \lambda (\omega^{n+1} - \omega^n) \\ & + \sum_{i=\pm} b_{hi}^{n+1} ((\mathbf{u}_{hi}^n - \mathbf{w}_{hi}^n) \circ (\phi_{h+}^n)^{-1}; \mathbf{u}_{hi}^{n+1}, \mathbf{v}_{hi}) \\ & + A_h^{n+1}(\mathbf{u}_h^n \circ (\phi_{h+}^n)^{-1}; \mathbf{u}_h^{n+1}, \mathbf{v}_h) + B_h^{n+1}(\mathbf{v}_h, p_h^{n+1}) - B_h^{n+1}(\mathbf{u}_h^{n+1}, q_h) = 0 \end{aligned} \quad (2.33c)$$

hold for any $(\mathbf{v}_h, q_h, \lambda) \in \mathcal{V}_k^{n+1} \times \mathcal{Q}_{k-1}^{n+1} \times \mathbb{R}$ that satisfies

$$\mathbf{v}_{h+}|_{\Gamma_{h+}^{n+1}} = \lambda \mathbf{v}^R|_{\Gamma_{h+}^{n+1}}, \quad \mathbf{v}_{h-}|_{\Gamma_{h-}^{n+1}} = 0. \quad (2.33d)$$

Remark 2.2. To handle the constraint (2.33b), we decompose the solution as:

$$\mathbf{u}_{h+}^{n+1} = \tilde{\mathbf{u}}_{h+}^{n+1} + \omega^{n+1} \mathbf{v}^R,$$

where ω^{n+1} is a scalar unknown and $\tilde{\mathbf{u}}_{h+}^{n+1}$ vanishes on Γ_{h+}^{n+1} . Then (2.33b) can then be reformulated as an unconstrained problem. We seek $(\tilde{\mathbf{u}}_h^{n+1}, p_h^{n+1}, \omega^{n+1}) \in \dot{\mathcal{V}}_k^{n+1} \times \mathcal{Q}_{k-1}^{n+1} \times \mathbb{R}$ such that (2.33c) is satisfied for two test function classes:

- Type I: any $(\mathbf{v}_h, q_h, 0) \in \dot{\mathcal{V}}_k^{n+1} \times \mathcal{Q}_{k-1}^{n+1} \times \mathbb{R}$
- Type II: $(\mathbf{v}_{h+}, \mathbf{v}_{h-}, q_h, \lambda) = (\mathbf{v}^R, 0, 0, 1)$.

To clarify the matrix assembly process while avoiding lengthy formulas, we focus on implementing the first two lines of (2.33c). The remaining terms follow standard assembly procedures.

Let us denote the nodal values of $(\tilde{\mathbf{u}}_{h+}^{n+1}, \tilde{\mathbf{u}}_{h-}^{n+1}, \mathbf{v}^R)$ as $(\tilde{U}_+^{n+1}, \tilde{U}_-^{n+1}, V^R)$, and denote the mass matrix of $\mathbf{V}_k(\Omega_{hi}^{n+1})$ as M_i^{n+1} . Note that the basis functions on Ω_{h+}^{n+1} can be pulled back to the basis functions on Ω_{h+}^n by ϕ_{h+}^n , $\tilde{\mathbf{u}}_{h+}^{n+1} \circ \phi_{h+}^n$ corresponds a finite element function in $\mathbf{V}_k(\Omega_{h+}^n)$ with nodal values \tilde{U}_+^{n+1} . By testing functions of Type I, the matrix-vector forms of $(\tilde{\mathbf{u}}_{h+}^{n+1}, \mathbf{v}_{h+})_{\Omega_{h+}^{n+1}}$ and $(\tilde{\mathbf{u}}_{h+}^{n+1} \circ \phi_{h+}^n, \mathbf{v}_{h+} \circ \phi_{h+}^n)_{\Omega_{h+}^n}$ are $M_+^{n+1} \tilde{U}_+^{n+1}$ and $M_+^n \tilde{U}_+^{n+1}$ respectively. By testing functions of Type II, the matrix-vector form of $(\tilde{\mathbf{u}}_{h+}^{n+1}, \mathbf{v}_{h+})_{\Omega_{h+}^{n+1}}$ writes $(M_+^{n+1} V^R)^T \tilde{U}_+^{n+1}$. Other terms can be expressed similarly. As a result, the first two

lines in (2.33c) can be written into the matrix-vector formulation:

$$\frac{1}{\tau} \begin{pmatrix} I_s + c^{n+1/2} (M_+^{n+1/2} V^R)^T & & \\ M_+^{n+1/2} V^R & M_+^{n+1/2} & \\ & & M_-^{n+1} \end{pmatrix} \begin{pmatrix} \omega^{n+1} \\ \tilde{U}_+^{n+1} \\ \tilde{U}_-^{n+1} \end{pmatrix} - \frac{1}{\tau} \begin{pmatrix} I_s + c^n (M_+^n V^R)^T & & \\ M_+^n V^R & M_+^n & \\ & & M_-^n \end{pmatrix} \begin{pmatrix} \omega^n \\ \tilde{U}_+^n \\ \tilde{U}_-^n \end{pmatrix}, \quad (2.34)$$

where $M_+^{n+1/2} := (M_+^{n+1} + M_+^n)/2$, $c^{n+1/2} = (V^R)^T M_+^{n+1/2} V^R$ and $c^n = (V^R)^T M_+^n V^R$. The first row in (2.34) refers to the equation obtained by testing the Type II test functions, while the other rows refer to testing the Type I test functions.

Remark 2.3. Modified schemes can be introduced by adjusting the bilinear forms A_h^n and B_h^n in (2.28)–(2.29). The first variant replaces the exact interface integral on Γ with numerical quadrature approximations on Γ . The second variant incorporates a continuity penalty term $\alpha h^{-1} \langle \llbracket \mathbf{u} \rrbracket, \llbracket \mathbf{v} \rrbracket \rangle_\Gamma$ into A_h^n with $\alpha > 0$. In general, we denote their bilinear forms as \tilde{A}_h^n and \tilde{B}_h^n . To be specific, we employ a quadrature rule with weights $\{s_k\}$ and nodes $\{x_k\} \subset \Gamma$, and define the practical inner product:

$$\langle f, g \rangle_h := \sum_k s_k f(x_k) g(x_k).$$

Then we have

$$\begin{aligned} \tilde{A}_h^n(\mathbf{z}; \mathbf{u}, \mathbf{v}) &:= (2\mu \mathbb{D} \mathbf{u}_i, \mathbb{D} \mathbf{v}_i)_{\Omega_{h_i}^n} + \frac{1}{2} \langle \{ \{ (\mathbf{z} \cdot \mathbf{n}) \mathbf{u} \} \}, \llbracket \mathbf{v} \rrbracket \rangle_h - \frac{1}{2} \langle \{ \{ (\mathbf{z} \cdot \mathbf{n}) \mathbf{v} \} \}, \llbracket \mathbf{u} \rrbracket \rangle_h \\ &\quad - 2\mu \langle \{ \{ \mathbb{D}(\mathbf{u}) \mathbf{n} \} \}, \llbracket \mathbf{v} \rrbracket \rangle_h + 2\mu \langle \{ \{ \mathbb{D}(\mathbf{v}) \mathbf{n} \} \}, \llbracket \mathbf{u} \rrbracket \rangle_h + \frac{\alpha}{h} \langle \llbracket \mathbf{u} \rrbracket, \llbracket \mathbf{v} \rrbracket \rangle_h. \end{aligned}$$

Crucially, it is direct to verify that the modification maintains the key inequality:

$$\tilde{A}_h^n(\mathbf{z}; \mathbf{u}, \mathbf{u}) \geq \sum_{i=\pm} (2\mu \mathbb{D} \mathbf{u}_i, \mathbb{D} \mathbf{u}_i)_{\Omega_{h_i}^n}. \quad (2.35)$$

Now, we present the main theoretic results of this paper, addressing the unique solvability of (2.32b) and (2.33b)–(2.33d), and the energy-dissipating properties.

Theorem 2.2. *The fully discrete scheme (2.32) for the Navier-Stokes equations on a moving domain is uniquely solvable. Moreover, if $\mathbf{w}_D = 0$ and $\mathbf{f} = 0$, we have*

$$\begin{aligned} \tilde{E}^{n+1} - \tilde{E}^n &= -2\mu\tau (\|\mathbb{D}(\mathbf{u}_{h+}^{n+1})\|_{\Omega_{h+}^{n+1}}^2 + \|\mathbb{D}(\mathbf{u}_{h-}^{n+1})\|_{\Omega_{h-}^n}^2) - \frac{1}{2} \|\mathbf{u}_{h+}^{n+1} \circ \phi_{h+}^n - \mathbf{u}_{h+}^n\|_{\Omega_{h+}^n}^2 \\ &\quad - \frac{1}{2} \|\mathbf{u}_{h-}^{n+1} - \mathbf{u}_{h-}^n\|_{\Omega_{h-}^n}^2 \leq 0, \end{aligned} \quad (2.36)$$

where \tilde{E}^n is defined as

$$\tilde{E}^n = \frac{1}{2} [\|\mathbf{u}_{h+}^n\|_{\Omega_{h+}^n}^2 + \|\mathbf{u}_{h-}^n\|_{\Omega_{h-}^n}^2]. \quad (2.37)$$

Theorem 2.3. *The fully discrete scheme (2.33) is uniquely solvable. Let \mathbf{u}_h^{n+1} , p_h^{n+1} , ω^{n+1} denote the numerical solutions at t_{n+1} . Then, the discrete energy-dissipation law is satisfied.*

$$\begin{aligned} E^{n+1} - E^n &= -2\mu\tau (\|\mathbb{D}(\mathbf{u}_{h+}^{n+1})\|_{\Omega_{h+}^{n+1}}^2 + \|\mathbb{D}(\mathbf{u}_{h-}^{n+1})\|_{\Omega_{h-}^n}^2) - \frac{1}{2} \|\mathbf{u}_{h+}^{n+1} \circ \phi_{h+}^n - \mathbf{u}_{h+}^n\|_{\Omega_{h+}^n}^2 \\ &\quad - \frac{1}{2} \|\mathbf{u}_{h-}^{n+1} - \mathbf{u}_{h-}^n\|_{\Omega_{h-}^n}^2 - \frac{I_s}{2\tau} (\omega^{n+1} - \omega^n)^2 \leq 0, \end{aligned} \quad (2.38)$$

where E^n is defined as

$$E^n = \frac{1}{2} [\|\mathbf{u}_{h+}^n\|_{\Omega_{h+}^n}^2 + \|\mathbf{u}_{h-}^n\|_{\Omega_{h-}^n}^2] + \frac{1}{2} I_s |\omega^n|^2. \quad (2.39)$$

3. Proofs of Theorems 2.2–2.3. Since (2.33) is a linear system, the uniqueness leads to the existence of solutions. The uniqueness of (2.32b) and (2.33b)–(2.33d) can be proved

based on the energy-dissipation properties (2.36) and (2.38) and the inf-sup condition of B_h^{n+1} in Theorem 3.1.

3.1. Proof of energy dissipation. We first present the proof of Theorem 2.3.

Proof. [Proof of (2.38)] Taking $(\mathbf{v}_h, q_h, \lambda) = (\mathbf{u}_h^{n+1}, p_h^{n+1}, \omega^{n+1})$ in (2.33b)–(2.33d). By using the skew-symmetric of $b_{hi}^{n+1}(\cdot; \cdot, \cdot)$ with respect to the last two entries, we get

$$\begin{aligned} & \frac{1}{2\tau} [\|\mathbf{u}_{h+}^{n+1}\|_{\Omega_{h+}^{n+1}}^2 - 2(\mathbf{u}_{h+}^n, \mathbf{u}_{h+}^{n+1} \circ \phi_{h+}^n)_{\Omega_{h+}^n} + \|\mathbf{u}_{h+}^{n+1} \circ \phi_{h+}^n\|_{\Omega_{h+}^n}^2] \\ & + \frac{1}{\tau} I_s \omega^{n+1} (\omega^{n+1} - \omega^n) + \frac{1}{\tau} (\mathbf{u}_{h-}^{n+1} - \mathbf{u}_{h-}^n, \mathbf{u}_{h-}^{n+1})_{\Omega_{h-}} + \sum_{i=\pm} (2\mu \mathbb{D}\mathbf{u}_{hi}^{n+1}, \mathbb{D}\mathbf{u}_{hi}^{n+1})_{\Omega_{hi}^{n+1}} = 0. \end{aligned} \quad (3.1)$$

Using $(a-b)a = \frac{1}{2}(a^2 - b^2) + \frac{1}{2}(a-b)^2$, we obtain

$$\begin{aligned} & \frac{1}{2\tau} [\|\mathbf{u}_{h+}^{n+1}\|_{\Omega_{h+}^{n+1}}^2 - \|\mathbf{u}_{h+}^n\|_{\Omega_{h+}^n}^2 + \|\mathbf{u}_{h+}^{n+1} \circ \phi_{h+}^n - \mathbf{u}_{h+}^n\|_{\Omega_{h+}^n}^2] \\ & + \frac{I_s}{2\tau} (|\omega^{n+1}|^2 - |\omega^n|^2 + (\omega^{n+1} - \omega^n)^2) + \sum_{i=\pm} (2\mu \mathbb{D}\mathbf{u}_{hi}^{n+1}, \mathbb{D}\mathbf{u}_{hi}^{n+1})_{\Omega_{hi}^{n+1}} \\ & + \frac{1}{2\tau} [\|\mathbf{u}_{h-}^{n+1}\|_{\Omega_{h-}^{n+1}}^2 - \|\mathbf{u}_{h-}^n\|_{\Omega_{h-}^n}^2 + \|\mathbf{u}_{h-}^{n+1} - \mathbf{u}_{h-}^n\|_{\Omega_{h-}^n}^2] = 0. \end{aligned} \quad (3.2)$$

This completes the proof of (2.38). \square

Remark 3.1. (2.36)–(2.37) in Theorem 2.2 can be proved similarly since the assumption $\mathbf{w}_D = 0$ leads to the equivalence of the test and the trial function spaces. The modified scheme introduced in Remark 2.3 maintains the energy-dissipation property. This follows from an analogous proof using the key inequality (2.35) and the inherent skew-symmetry of the formulation.

Theorem 3.1. *The following inf-sup condition holds true for all n ,*

$$\sup_{\mathbf{v}_h \neq 0 \in \dot{\mathbf{V}}_k^{n+1}} \frac{B_h^{n+1}(\mathbf{v}_h, q_h)}{|\mathbf{v}_h|_1} \gtrsim \|q_h\|_{L^2}, \quad \forall q_h \in \mathcal{Q}_{k-1}^{n+1}.$$

Remark 3.2. In the following proof, we focus on the two-dimensional case for simplicity of geometrical description. The proof for the cylindrical artificial interface in three dimensions proceeds similarly, with some additional details noted in Remarks 3.3.

The proof of Theorem 3.1 relies on the following lemmas.

Lemma 3.2. *There exists a constant $C > 0$ such that for any $q_h \in \mathcal{Q}_{k-1}(\Omega_{h+}^{n+1}) \times \mathcal{Q}_{k-1}(\Omega_{h-}^{n+1})$ (see (2.20)), there exists $\mathbf{v}_h \in \dot{\mathbf{V}}_k(\Omega_{h+}^{n+1}) \times \dot{\mathbf{V}}_k(\Omega_{h-}^{n+1})$ (see (2.18)) satisfying the following estimates:*

$$|\mathbf{v}_h|_1 \leq C \|q_h\|_{L^2}, \quad \|q_h\|_{L^2}^2 \leq C B_h^{n+1}(\mathbf{v}_h, q_h). \quad (3.3)$$

Proof. According to the inf-sup conditions (2.21) on subdomains, there exists $\tilde{\mathbf{v}}_{hi} \in \dot{\mathbf{V}}_k(\Omega_{hi}^{n+1})$ such that

$$\|q_{hi}\|_{L^2(\Omega_{hi}^{n+1})} \lesssim \frac{(\nabla \cdot \tilde{\mathbf{v}}_{hi}, q_{hi})_{\Omega_{hi}^{n+1}}}{\|\tilde{\mathbf{v}}_{hi}\|_{H^1(\Omega_{hi}^{n+1})}}.$$

Then we choose $\mathbf{v}_{hi} = -c\tilde{\mathbf{v}}_{hi}$ with $c = \|q_{hi}\|_{L^2(\Omega_{hi}^{n+1})} / \|\nabla \tilde{\mathbf{v}}_{hi}\|_{L^2(\Omega_{hi}^{n+1})}$ to obtain

$$\|\nabla \mathbf{v}_{hi}\|_{L^2(\Omega_{hi}^{n+1})} = \|q_{hi}\|_{L^2(\Omega_{hi}^{n+1})}, \quad (3.4)$$

$$\|q_{hi}\|_{L^2(\Omega_{hi}^{n+1})}^2 \lesssim - \int_{\Omega_{hi}^{n+1}} \nabla \cdot \mathbf{v}_{hi} q_{hi}. \quad (3.5)$$

Now we are going to prove $\mathbf{v}_h = (\mathbf{v}_{h+}, \mathbf{v}_{h-})$ satisfies (3.3). Note that $\mathbf{v}_{hi}|_{\Gamma_{hi}^{A,n+1}} = 0$ and $\text{dist}(\Gamma_{hi}^{A,n+1}, \Gamma) \lesssim h^{m+1}$, by the mean value theorem, the inverse inequality, and (3.4), we obtain

$$\|\mathbf{v}_{hi}\|_{L^2(\Gamma)} \lesssim \|\mathbf{v}_{hi}\|_{L^\infty(\Gamma)} \lesssim h^{m+1} \|\nabla \mathbf{v}_{hi}\|_{L^\infty(\Omega_{hi}^{n+1})} \lesssim h^{m+1-d/2} \|\nabla \mathbf{v}_{hi}\|_{L^2(\Omega_{hi}^{n+1})}. \quad (3.6)$$

Thus, for $m \geq 1$, we obtain

$$|\mathbf{v}_h|_1 \lesssim \sum_{i=\pm} \|\nabla \mathbf{v}_{hi}\|_{L^2(\Omega_{hi}^{n+1})} + h^{-1/2} \|\mathbf{v}_{hi}\|_{L^2(\Gamma)} \lesssim \sum_{i=\pm} \|q_{hi}\|_{L^2(\Omega_{hi}^{n+1})}.$$

In addition, using trace inequality leads to

$$\langle \{\{q_h \mathbf{n}\}\}, \llbracket \mathbf{v}_h \rrbracket \rangle_\Gamma \lesssim h^{-1/2} \max_{i=\pm} \|q_{hi}\|_{L^2(\Omega_{hi}^{n+1})} \max_{i=\pm} \|\mathbf{v}_{hi}\|_{L^2(\Gamma)} \lesssim h^{1/2} \|q_h\|_{L^2}^2, \quad (3.7)$$

where the last line can be proved for $d = 2$ by using (3.4) and (3.6) and for $d = 3$ by using Remark 3.3. Thus, by choosing h sufficiently small, we have

$$B_h^{n+1}(q_h, \mathbf{v}_h) = - \sum_{i=\pm} (\operatorname{div} \mathbf{v}_{hi}, q_{hi})_{\Omega_{hi}^{n+1}} + \langle \{\{q_h \mathbf{n}\}\}, \llbracket \mathbf{v}_h \rrbracket \rangle_\Gamma \geq (c - h^{1/2}) \|q_h\|_{L^2}^2 \geq c \|q_h\|_{L^2}^2.$$

□

Remark 3.3. For the cylindrical artificial interface where $d = 3$, the same proof can work for $m \geq 2$ by using (3.6). For $d = 3$ and $m = 1$, we should refine the estimate of $\|\mathbf{v}_{hi}\|_{L^2(\Gamma)}$ in the following way. Note that the cylindrical artificial interface consists of the top and the bottom bases and the lateral surface. Since the top and the bottom bases are flat, no geometric discrepancy is involved and thus both $\mathbf{v}_{h\pm}$ vanish. Next, we consider the boundary element K with a face F that approximates \tilde{F} on the lateral surface. Assume F lies on the $x_1 - x_2$ plane and \tilde{F} is described as a graph $(x_1, x_2, \phi(x_1, x_2))$. Denote the lift function from F to \tilde{F} as φ such that $\varphi((x_1, x_2, 0)) = (x_1, x_2, \phi(x_1, x_2))$. Then $|\varphi(x) - x| \leq h^2$ for $x \in F$ and $\det(D\varphi) = 1 + \mathcal{O}(h^2)$. Thus, using $\mathbf{v}_{hi} = 0$ on F ,

$$\begin{aligned} \|\mathbf{v}_{hi}\|_{L^2(\tilde{F})}^2 &\lesssim \int_F \left| \int_0^{\phi(x_1, x_2)} \partial_{x_3} \mathbf{v}_{hi} dx_3 \right|^2 dx_1 dx_2 \\ &\lesssim \int_F |\phi(x_1, x_2)| \int_0^{\phi(x_1, x_2)} |\nabla \mathbf{v}_{hi}|^2 dx_3 dx_1 dx_2 \\ &\lesssim \sup_{x \in F} |\varphi(x) - x| \|\nabla \mathbf{v}_{hi}\|_{L^2(K)}^2. \end{aligned}$$

By summing up the boundary elements, we obtain

$$\|\mathbf{v}_{hi}\|_{L^2(\Gamma)} \lesssim h \|\nabla \mathbf{v}_{hi}\|_{L^2(\Omega_{hi}^{n+1})}. \quad (3.8)$$

Lemma 3.3. Let P_h^* denote a one dimensional linear subspace of \mathbb{R}^2 ,

$$P_h^* = \{(p_{h+}, p_{h-}) \in \mathbb{R}^2 : p_{h+} |\Omega_{h+}^{n+1}| + p_{h-} |\Omega_{h-}^{n+1}| = 0\}. \quad (3.9)$$

There exist $h_0 > 0$ and $C > 0$ such that for $h \leq h_0$ and any $p_h \in P_h^*$, there exist functions $\mathbf{v}_{h+} \in \mathbf{V}_k(\Omega_{h+}^{n+1})$ and $\mathbf{v}_{h-} \in \mathbf{V}_k(\Omega_{h-}^{n+1})$, such that

$$\mathbf{v}_{h+}|_{\Gamma_{h+}^{n+1}} = 0, \quad \mathbf{v}_{h-}|_{\Gamma_{h-}^{n+1}} = 0,$$

and $\mathbf{v}_h = (\mathbf{v}_{h+}, \mathbf{v}_{h-})$ satisfies

$$|\mathbf{v}_h|_1 \leq C \|p_h\|_{L^2}, \quad \|p_h\|_{L^2}^2 \leq C B_h^{n+1}(\mathbf{v}_h, p_h). \quad (3.10)$$

Proof. We first assume the existence of smooth functions \mathbf{g}_i on Ω_i for $i = \pm$ such that $\mathbf{g}_i|_{\Gamma_i} = 0$ and

$$\begin{aligned} \mathbf{g}_+|_{A_{+,\delta}} &= \mathbf{g}, \quad A_{+,\delta} := \{(x_1, x_2, x_3) : 1 - \delta \leq x_1^2 + x_2^2 \leq 1\}, \\ \mathbf{g}_-|_{A_{-,\delta}} &= \mathbf{g}, \quad A_{-,\delta} := \{(x_1, x_2, x_3) : 1 \leq x_1^2 + x_2^2 \leq 1 + \delta\}, \end{aligned}$$

for $\mathbf{g} = (x_1, x_2, 0)^T$ and some $\delta < 1$. For 2 dimensional case, \mathbf{g} contains only the first two components. Such smooth functions can be easily constructed as a radial function. We emphasize that \mathbf{g} is equal to the unit exterior normal vector field n_Γ of Γ .

We are going to prove that the following choice of $\mathbf{v}_h = (\mathbf{v}_{h+}, \mathbf{v}_{h-})$ satisfies (3.10),

$$\mathbf{v}_{hi} = (|\Omega_{h-}^{n+1}| p_{h-} - |\Omega_{h+}^{n+1}| p_{h+}) I_{hi} \mathbf{g}_i, \quad i = \pm,$$

where I_{hi} denotes the interpolation with respect to $\mathbf{V}_k(\Omega_{hi}^{n+1})$. Via the definition of inter-

polation, it is direct to deduce the following boundary behaviour. First, $\mathbf{v}_{hi} \in \mathbf{V}_k(\Omega_{hi}^{n+1})$ and vanishes on Γ_{hi}^{n+1} . Second, for $h < \delta/4$, $A_{i,\delta}$ covers the layer of elements adjacent to Γ in Ω_{hi}^{n+1} . Consequently, \mathbf{g}_i is linear in $A_{i,\delta}$ and the interpolation $I_{hi}\mathbf{g}_i$ exactly matches \mathbf{g} within this layer. This property also works for the case of the high-order isoparametric finite elements, see [24, P. 3 (4)] and Remark 2.1. By extension, we obtain $I_{hi}\mathbf{g}_i|_\Gamma = \mathbf{n}_\Gamma$. In consequence,

$$\llbracket \mathbf{v}_h \rrbracket = 0. \quad (3.11)$$

By H^1 stability of the interpolation, we have

$$\|\mathbf{v}_h\|_1^2 = (|\Omega_{h-}^{n+1}|p_{h-} - |\Omega_{h+}^{n+1}|p_{h+})^2 \sum_{i=\pm} \|\nabla I_{hi}\mathbf{g}_i\|_{L^2(\Omega_{hi}^{n+1})}^2 \lesssim \|p_h\|_{L^2}^2.$$

Furthermore, using (3.11), the Stokes theorem, and p_{hi} is constant, we obtain

$$\begin{aligned} B_h^{n+1}(\mathbf{v}_h, p_h) &= - \sum_i p_{hi} \int_{\Omega_{hi}^{n+1}} \operatorname{div} \mathbf{v}_{hi} \\ &= (|\Omega_{h-}^{n+1}|p_{h-} - |\Omega_{h+}^{n+1}|p_{h+}) \sum_{i=\pm} p_{hi} \int_{\Gamma_{hi}^{A,n+1}} \mathbf{g} \cdot \mathbf{n}_{hi}, \end{aligned}$$

where \mathbf{n}_{hi} denotes the exterior normal vector of $\Gamma_{hi}^{A,n+1}$. According to [17, Prop. 2.3] and noticing that the orientation of Ω_{h-}^{n+1} , we have

$$\|\mathbf{n}_{h+} - \mathbf{g}\|_{L^\infty(\Gamma_{h+}^{A,n+1})} \lesssim h^m, \quad \|\mathbf{n}_{h-} + \mathbf{g}\|_{L^\infty(\Gamma_{h-}^{A,n+1})} \lesssim h^m.$$

Since $\operatorname{dist}(\Gamma_{hi}^{A,n+1}, \Gamma) \lesssim h^{m+1}$, we obtain

$$\begin{aligned} \int_{\Gamma_{h+}^{A,n+1}} \mathbf{g} \cdot \mathbf{n}_{h+} &= \int_{\Gamma_{h+}^{A,n+1}} x_1^2 + x_2^2 + \mathcal{O}(h^m) = 2\pi + \mathcal{O}(h^m), \\ \int_{\Gamma_{h-}^{A,n+1}} \mathbf{g} \cdot \mathbf{n}_{h-} &= \int_{\Gamma_{h-}^{A,n+1}} -(x_1^2 + x_2^2) + \mathcal{O}(h^m) = -2\pi + \mathcal{O}(h^m). \end{aligned}$$

Thus,

$$B_h^{n+1}(\mathbf{v}_h, p_h) \geq 2\pi(p_{h+} - p_{h-})(|\Omega_{h-}^{n+1}|p_{h-} - |\Omega_{h+}^{n+1}|p_{h+}) - ch^m \|p_h\|_{L^2}^2.$$

Further, for the first term, after introducing

$$D = \begin{pmatrix} |\Omega_{h+}^{n+1}| & 0 \\ 0 & |\Omega_{h-}^{n+1}| \end{pmatrix}, \quad B = \begin{pmatrix} -1 & 1 \\ 1 & -1 \end{pmatrix},$$

we have

$$(p_{h+} - p_{h-})(|\Omega_{h-}^{n+1}|p_{h-} - |\Omega_{h+}^{n+1}|p_{h+}) = p_h^T D B p_h = q^T \hat{B} q,$$

where $\hat{B} = D^{1/2} B D^{-1/2}$ and $q = D^{1/2} p_h$. Since \hat{B} is similar to the semi-positive definite matrix B , it has two eigenvalues 0 and 2 and the null space $N(\hat{B})$ is spanned by $D^{1/2} e_1$ with $e_1 = (1, 1)^T$. Now, using $p_h \in P_h^*$ leads to

$$(q, D^{1/2} e_1) = (p_h, D e_1) = p_{h+} |\Omega_{h+}^{n+1}| + p_{h-} |\Omega_{h-}^{n+1}| = 0,$$

meaning that $q \in N(\hat{B})^\perp$. Thus,

$$q^T \hat{B} q \geq 2q^T q = 2\|p_h\|_{L^2}^2.$$

Thus, choosing h sufficiently small (independent of p), we conclude that

$$B_h^{n+1}(\mathbf{v}_h, p_h) \geq 2\pi \|p_h\|_{L^2}^2.$$

□

Proof. [Proof of Theorem 3.1] For any $p_h \in \mathcal{Q}_{k-1}^{n+1}$, we perform the following decomposition to its components: $p_{hi} = \tilde{p}_{hi} + \bar{p}_{hi}$ such that \bar{p}_{hi} are constants and

$$\int_{\Omega_{hi}^{n+1}} \tilde{p}_{hi} = 0, \quad (3.12)$$

which means \bar{p}_{hi} and \tilde{p}_{hi} are orthogonal in the L^2 inner product. According to (2.27), $\bar{p}_h = (\bar{p}_{h+}, \bar{p}_{h-}) \in P_h^*$. Applying Lemma 3.2–Lemma 3.3, we have $\tilde{\mathbf{v}}_h$ and $\bar{\mathbf{v}}_h$ such that

$$|\tilde{\mathbf{v}}_h|_1 \leq C_0 \|\tilde{p}_h\|_{L^2}, \quad \|\tilde{p}_h\|_{L^2}^2 \leq C_0 B_h^{n+1}(\tilde{\mathbf{v}}_h, \tilde{p}_h), \quad (3.13)$$

$$|\bar{\mathbf{v}}_h|_1 \leq C_0 \|\bar{p}_h\|_{L^2}, \quad \|\bar{p}_h\|_{L^2}^2 \leq C_0 B_h^{n+1}(\bar{\mathbf{v}}_h, \bar{p}_h). \quad (3.14)$$

Further, since \bar{p}_{hi} is constant and $\tilde{\mathbf{v}}_{hi} \in H_0^1(\Omega_{hi}^{n+1})$, by integration by parts and (3.6)–(3.8), we obtain

$$\begin{aligned} |B_h^{n+1}(\tilde{\mathbf{v}}_h, \bar{p}_h)| &= |\langle \{\{\bar{p}_h\}\}, \llbracket \tilde{\mathbf{v}}_h \rrbracket \cdot \mathbf{n} \rangle_{\Gamma}| \lesssim \max_{i=\pm} \|\bar{p}_{hi}\|_{L^2(\Gamma)} \max_{i=\pm} \|\tilde{\mathbf{v}}_{hi}\|_{L^2(\Gamma)} \\ &\lesssim h \|\bar{p}_h\|_{L^2} \max_{i=\pm} \|\nabla \tilde{\mathbf{v}}_{hi}\|_{L^2(\Omega_{hi}^{n+1})} \leq ch (\|\bar{p}_h\|_{L^2}^2 + \|\tilde{p}_h\|_{L^2}^2). \end{aligned} \quad (3.15)$$

By boundedness of B_h^{n+1} (using trace inequality and the penalty term in $|\cdot|_1$), we obtain

$$B_h^{n+1}(\tilde{\mathbf{v}}_h, \tilde{p}_h) \leq c_0 |\tilde{\mathbf{v}}_h|_1 \|\tilde{p}_h\|_{L^2}. \quad (3.16)$$

Then we consider $\mathbf{v}_h = (\mathbf{v}_{h+}, \mathbf{v}_{h-})$ with $\mathbf{v}_{hi} = \tilde{\mathbf{v}}_{hi} + \gamma \bar{\mathbf{v}}_{hi}$ with $\gamma = c_0^{-2} C_0^{-4}/4$. Then we get

$$|\mathbf{v}_h|_1^2 \lesssim |\tilde{\mathbf{v}}_h|_1^2 + |\bar{\mathbf{v}}_h|_1^2 \lesssim \|p_h\|_{L^2}^2.$$

Collecting (3.13)–(3.16), we obtain

$$\begin{aligned} B_h^{n+1}(\mathbf{v}_h, p_h) &= B_h^{n+1}(\tilde{\mathbf{v}}_h, \tilde{p}_h) + \gamma B_h^{n+1}(\bar{\mathbf{v}}_h, \bar{p}_h) + \gamma B_h^{n+1}(\tilde{\mathbf{v}}_h, \tilde{p}_h) + B_h^{n+1}(\tilde{\mathbf{v}}_h, \bar{p}_h) \\ &\geq C_0^{-1} \|\tilde{p}_h\|_{L^2}^2 + C_0^{-1} \gamma \|\bar{p}_h\|_{L^2}^2 - c_0 \gamma |\bar{\mathbf{v}}_h|_1 \|\tilde{p}_h\|_{L^2} - ch (\|\bar{p}_h\|_{L^2}^2 + \|\tilde{p}_h\|_{L^2}^2). \end{aligned}$$

Combining with

$$c_0 \gamma |\bar{\mathbf{v}}_h|_1 \|\tilde{p}_h\|_{L^2} \leq \frac{1}{4} \gamma C_0^{-1} \|\bar{p}_h\|_{L^2}^2 + c_0^2 \gamma C_0^3 \|\tilde{p}_h\|_{L^2}^2,$$

and choosing h sufficiently small, we obtain

$$B_h^{n+1}(\mathbf{v}_h, p_h) \geq (2C_0)^{-1} \|\tilde{p}_h\|_{L^2}^2 + (2C_0)^{-1} \gamma \|\bar{p}_h\|_{L^2}^2.$$

This ends the proof. \square

Proof. [Proof of Theorem 2.2–2.3] We first prove the unique solvability of (2.33b)–(2.33d). According to Remark 2.2, (2.33b)–(2.33d) is a linear system. Thus, it suffices to prove the uniqueness of solutions. The uniqueness of the velocity \mathbf{u}_h^{n+1} and ω^{n+1} can be proved by using the energy dissipating property (2.38). Then the inf-sup condition in Theorem 3.1 leads to the uniqueness of p_h^{n+1} . This ends the proof of Theorem 2.3.

For the Dirichlet problem, the proof for the uniqueness of solution is similar. Suppose there are two solutions $(\mathbf{u}_h^{n+1}, p_h^{n+1})$ and $(\tilde{\mathbf{u}}_h^{n+1}, \tilde{p}_h^{n+1})$ of (2.32b). Since (2.32b) is linear, the difference of these two solutions satisfies the same equation with vanishing \mathbf{f} and Dirichlet boundary conditions. According to Theorem 2.2 and Remark 3.1, we obtain the uniqueness of the velocity, while the uniqueness of the pressure can be obtained from Theorem 3.1. \square

4. Numerical examples. In this section, we present numerical examples to demonstrate the convergence rates of the proposed method and validate the energy-dissipating property obtained in Theorem 2.3. The proposed numerical scheme is implemented by the open sourced high performance Python package: NGSolve; see <https://ngsolve.org>.

4.1. Convergence tests. In this section, we apply the proposed scheme on the Navier-Stokes equations on a moving domain with Dirichlet boundary conditions to validate its convergence rates. The moving domain is enclosed by a rotating interior boundary and a fixed rectangular boundary of $[-1.5, 1.5] \times [-1.5, 1.5]$. For convenience of error measurement, we consider an example with manufactured exact solutions. To ensure the smoothness of the exact solutions, we consider the interior boundary which is described as the zero level set of $\phi(x, y, t)$ defined by

$$\begin{aligned} \phi(x, y, t) &= k^8 (x^2 + y^2)^3 - 0.01k^2 \\ &\quad - k^4 a^2 (x \cos(\omega t) + y \sin(\omega t))^2 (-x \sin(\omega t) + y \cos(\omega t))^2. \end{aligned}$$

The parameter ω describes the angular velocity and is set to be π . The other shape parameters are chosen as $k = 1.5$, $a = 3$, and $\mu = 1$. The geometric setting is demonstrated

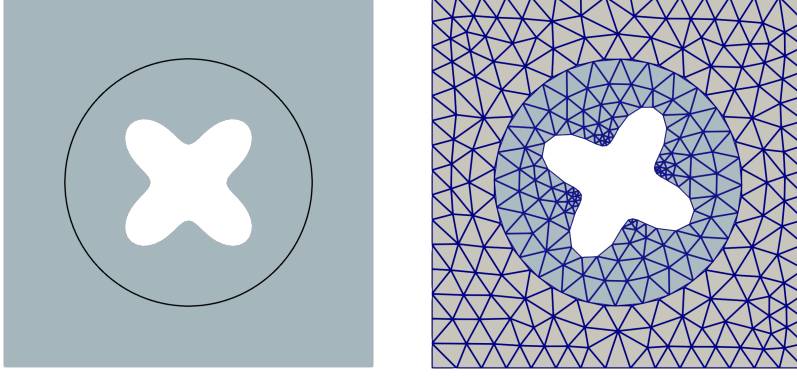


Fig. 4.1: Geometric setting and the sliding interface (convergence tests).

in Fig. 4.1. The mesh at $T = 0.1$ is demonstrated in the right panel of Fig. 4.1, where the rotating mesh and the stationary mesh have overlap near the artificial circular interface. The exact velocity field and the exact pressure are given as follows,

$$\mathbf{u}(x, y, t) = \omega \begin{pmatrix} -y \\ x \end{pmatrix} + g \begin{pmatrix} g_y \\ -g_x \end{pmatrix}, \quad p(x, y, t) = \phi(x, y, 0)x \exp(-2(x^2 + y^2)),$$

where $g(x, y, t) = \phi(x, y, t)(x^2 - 1.5^2)(y^2 - 1.5^2) \exp(-6(x^2 + y^2))$. It is obvious that u satisfies the incompressible condition and the Dirichlet boundary condition on the rotating interior boundary. According to the exact solutions of u and p , we determine the initial value u_0 and the right-hand side f correspondingly. The artificial interface is set at the circle with radius $R_I = 1$.

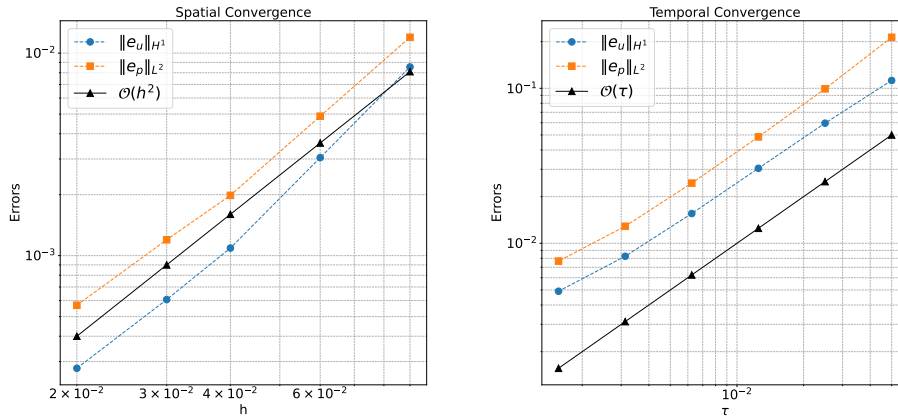


Fig. 4.2: Errors of spatial and temporal discretizations

On each subdomain, we use the P2-P1 element for spatial discretization which satisfies the inf-sup conditions on subdomains. To investigate the spatial convergence rate of the

proposed method, we choose $T = 3$ and a sufficiently small time stepsize $\tau = T/20000$. As demonstrated in Fig. 4.2, both the velocity error in H^1 norm and the pressure error in L^2 norm exhibit a second order convergence. The temporal convergence is tested with $T = 3$ and a small mesh size $h = 0.06$. The first order temporal convergence rates of both the velocity error in H^1 and the pressure error in L^2 are validated in Fig. 4.2. As discussed in Section 2.4, geometric approximation errors are involved in the proposed method. However, this numerical experiment confirms that P2-P1 Taylor-Hood elements on straight-edged triangulations achieve optimal convergence rates despite these errors.

4.2. Motion of the fluid driven by a forced rotator. In this section, we apply the proposed scheme (2.32) to simulate the motion of the fluid driven by a slender four-blade propeller with a given velocity. In this example, we set $\mu = 0.01$. The Dirichlet boundary condition in (2.7d) is set by $\mathbf{w}_D = \omega(t)\mathbf{v}_{\Gamma_+(t)}$ with

$$\omega(t) = \begin{cases} t, & t < 2, \\ 2, & t \geq 2. \end{cases}$$

The geometric setting together with the computational mesh are illustrated in Fig 4.3.

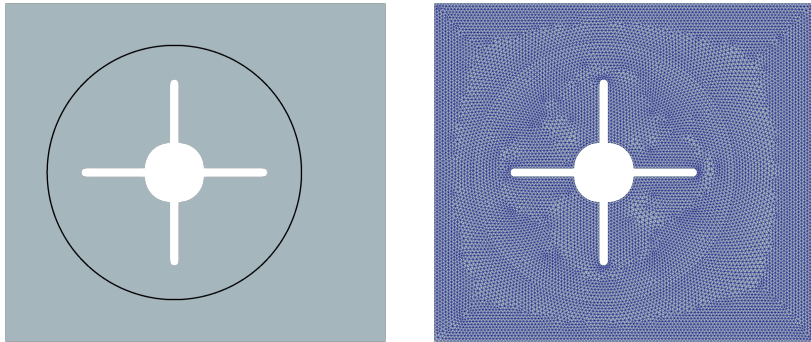


Fig. 4.3: Sliding interface and computational mesh (example of forced rotator).

Compared with the first case where the interior boundary is smoother, slender blades typically induce stronger vortex effects in the fluid motion. This is because of the sudden changes in flow direction at the corners, which leads to the generation of strong vortices.

As demonstrated in Fig. 4.4a–4.4b, at the beginning several rotations, the pressure rapidly increases in front of the blades (windward side) due to the fact that the fluid has been pushed, creating a high-pressure zone. Conversely, behind the blades (in the wake region), the fluid is pulled, leading to a drop in pressure and forming a low-pressure zone. Around the blades, the pressure gradient becomes pronounced.

Under the influence of the rotating blades, see in Fig. 4.4c–4.4d, the fluid continuously accelerates. The centrifugal force causes the pressure to be lower in the central region of the cavity, while it becomes higher near the cavity’s outer edges (close to the walls). As time progresses, due to the no-slip boundary condition, the pressure near the cavity walls gradually increases. This occurs because the fluid is decelerated as it approaches the walls, leading to the build-up of the pressure.

4.3. Energy dissipation of the FSI problem. In this section, we validate the energy-dissipating property of the proposed fully discrete scheme (2.33) for the FSI problem. The FSI problem considered here is the continuation of the movement of the four-blade

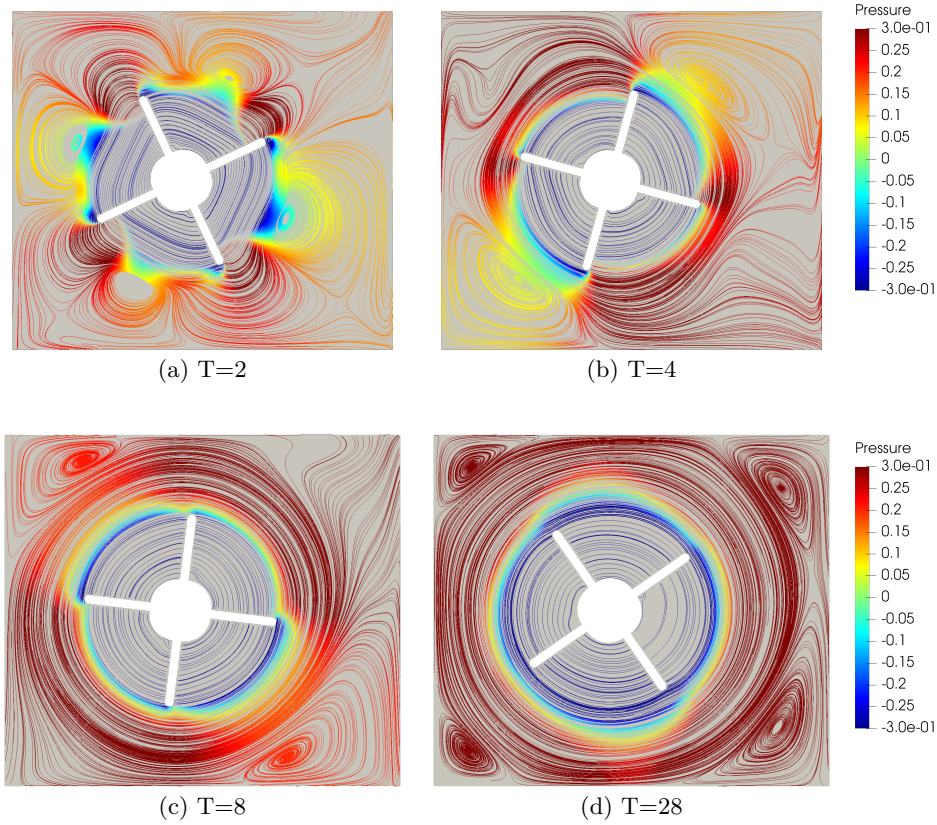


Fig. 4.4: Streamlines and pressure field (example of forced rotator)

propeller from the previous section after $T = 30$, but without any driving force applied to the rotating structure. This allows for the free interaction between the rotating propeller and the fluid. In other words, we solve (2.33) with initial velocity field and the geometry set by the solution of the previous section at $T = 30$, which is demonstrated in Fig 4.6a. Thus, the initial velocity field weakly satisfies the incompressible condition and we continue the time counting, meaning $T = 30$ is the starting time of FSI.

After the driving force is removed, the slender four-blade propeller will continue to rotate due to inertia. As the viscous forces of the fluid exert resistance on the propeller, its angular speed ω will gradually decrease, as validated in Fig 4.5.

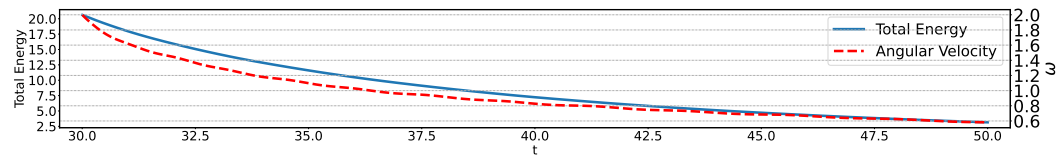


Fig. 4.5: Decay of angular velocity and total energy (FSI with a rotating rigid structure)

We present several snapshots of the streamlines of the fluid field at different times in Fig 4.6a-Fig 4.6d. After the removal of the driving force, the flow field will gradually evolve

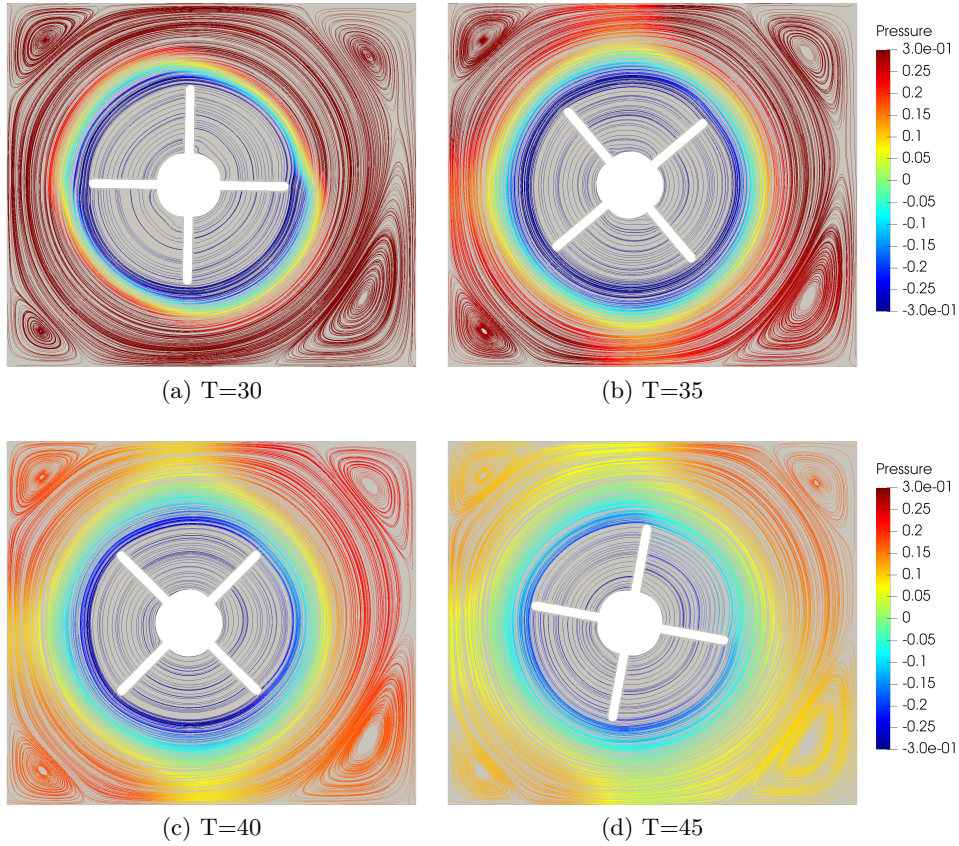


Fig. 4.6: Streamlines and pressure field (FSI with a rotating rigid structure)

from active movement to a state of rest. Initially, the flow shows significant velocity and pressure magnitudes. As the propeller slows down, the velocity field becomes less dynamic. The system's total kinetic energy decreases over time, as evidenced in Fig 4.5.

Finally, we illustrate the energy dissipation between consecutive time steps in Fig 4.7. According to Theorem 2.3, the total energy should always decrease. Fig 4.7 demonstrates that $E^{n+1} - E^n \leq 0$, which is consistent with the theoretical analysis, and validates the effectiveness of the proposed method in preserving the energy dissipation of the original FSI problem. Because of the energy-dissipating property, the proposed method is robust for long time simulation for FSI problems with a rotating rigid structure.

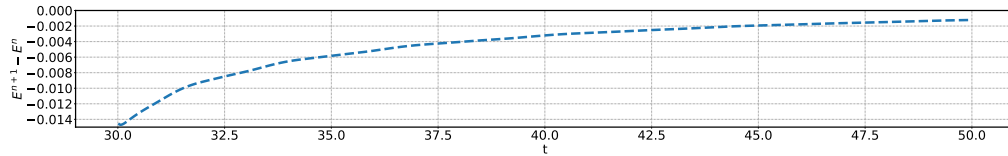


Fig. 4.7: Energy dissipation (FSI with a rotating rigid structure)

5. Conclusion. In this paper, we have proposed a fully discrete energy dissipating scheme for simulating the fluid-structure interaction with a rotating rigid structure in

the framework of the sliding interface method. A skew-symmetric Nitsche’s stabilization term on the artificial sliding interface, alongside a rotational arbitrary Lagrangian–Eulerian framework have been employed to preserve the energy-dissipating property at the continuous level and to guarantee the good mesh quality simultaneously. At the discrete level, a first order fully discretization has been proposed and proved to preserve the energy-dissipating property. Moreover, the inf-sup condition has been proved for Taylor-Hood type elements on non-matching or overlapping sub-meshes, leading to the applicability and robustness of the proposed approach. Based on the energy dissipating property and the inf-sup condition, the unique solvability of the fully discrete scheme has been proved. The accuracy and the energy-dissipation law of proposed method have been validated by extensive numerical examples.

REFERENCES

- [1] S. BADIA AND R. CODINA, *Analysis of a stabilized finite element approximation of the transient convection-diffusion equation using an ALE framework*, SIAM J. Numer. Anal., 44 (2006), pp. 2159–2197, <https://doi.org/10.1137/050643532>.
- [2] J. BARRETT, H. GARCKE, AND R. NÜRNBERG, *A stable parametric finite element discretization of two-phase Navier–Stokes flow*, J. Sci. Comput., 63 (2015), pp. 78–117, <https://doi.org/10.1007/s10915-014-9885-2>.
- [3] C. BAUMANN AND J. ODEN, *A discontinuous hp finite element method for convection-diffusion problems*, Comput. Methods Appl. Mech. Engrg., 175 (1999), pp. 311–341.
- [4] C. BAUMANN AND J. ODEN, *A discontinuous hp finite element method for the Euler and Navier–Stokes equations*, Int. J. Numer. Methods Fluids, 31 (1999), pp. 79–95.
- [5] Y. BAZILEVS, M.-C. HSU, I. AKKERMAN, S. WRIGHT, K. TAKIZAWA, B. HENICKE, T. SPIELMAN, AND T. E. TEZDUYAR, *3D simulation of wind turbine rotors at full scale. Part I: Geometry modeling and aerodynamics*, Int. J. Numer. Methods Fluids, 65 (2011), pp. 207–235, <https://doi.org/10.1002/flid.2400>.
- [6] Y. BAZILEVS, M.-C. HSU, J. KIENDL, R. WÜCHNER, AND K.-U. BLETZINGER, *3D simulation of wind turbine rotors at full scale. Part II: Fluid–structure interaction modeling with composite blades*, Int. J. Numer. Methods Fluids, 65 (2011), pp. 236–253, <https://doi.org/10.1002/flid.2454>.
- [7] Y. BAZILEVS, M.-C. HSU, AND M. A. SCOTT, *Isogeometric fluid–structure interaction analysis with emphasis on non-matching discretizations, and with application to wind turbines*, Comput. Methods Appl. Mech. Eng., 249–252 (2012), pp. 28–41, <https://doi.org/10.1016/j.cma.2012.03.028>.
- [8] Y. BAZILEVS, M.-C. HSU, K. TAKIZAWA, AND T. E. TEZDUYAR, *ALE-VMS and ST-VMS methods for computer modeling of wind-turbine rotor aerodynamics and fluid–structure interaction*, Math. Models Methods Appl. Sci., 22 (2012), p. 1230002, <https://doi.org/10.1142/S0218202512300025>.
- [9] Y. BAZILEVS AND T. HUGHES, *NURBS-based isogeometric analysis for the computation of flows about rotating components*, Comput. Mech., 43 (2008), pp. 143–150, <https://doi.org/10.1007/s00466-008-0277-z>.
- [10] M. BEHR AND T. TEZDUYAR, *Shear-slip mesh update in 3D computation of complex flow problems with rotating mechanical components*, Comput. Methods Appl. Mech. Eng., 190 (2001), pp. 3189–3200, [https://doi.org/10.1016/S0045-7825\(00\)00388-1](https://doi.org/10.1016/S0045-7825(00)00388-1).
- [11] D. BOFFI, F. BREZZI, AND M. FORTIN, *Mixed Finite Element Methods and Applications*, vol. 44 of Springer Series in Computational Mathematics, Springer, 2013, <https://doi.org/10.1007/978-3-642-36519-5>.
- [12] D. BOFFI AND L. GASTALDI, *Stability and geometric conservation laws for ALE formulation*, Comput. Methods Appl. Mech. Eng., 193 (2004), pp. 4717–4739, <https://doi.org/10.1016/j.cma.2004.02.020>.
- [13] J. M. BOLAND AND R. A. NICOLAIDES, *Stability of finite elements under divergence constraints*, SIAM J. Numer. Anal., 20 (1983), pp. 722–731, <https://doi.org/10.1137/0720048>.
- [14] A. BRESSAN, *Isogeometric regular discretization for the Stokes problem*, IMA J. Numer. Anal., 31 (2011), pp. 1334–1356, <https://doi.org/10.1093/imanum/drq014>.
- [15] V. M. CALO, N. F. BRASHER, Y. BAZILEVS, AND T. J. R. HUGHES, *Multiphysics model for blood flow and drug transport with application to patient-specific coronary artery flow*, Comput Mech, 43 (2008), pp. 161–177, <https://doi.org/10.1007/s00466-008-0321-z>.
- [16] A. CORSINI, F. RISPOLI, AND T. TEZDUYAR, *Stabilized finite element computation of NOx emission in aero-engine combustors*, Int. J. Numer. Methods Fluids, 65 (2011), pp. 254–270, <https://doi.org/10.1002/flid.2451>.
- [17] A. DEMLOW, *Higher-order finite element methods and pointwise error estimates for elliptic problems on surfaces*, SIAM J. Numer. Anal., 47 (2009), pp. 805–827, <https://doi.org/10.1137/>

- 070708135.
- [18] B. DUAN, B. LI, AND Z. YANG, *An energy diminishing arbitrary Lagrangian–Eulerian finite element method for two-phase Navier–Stokes flow*, *J. Comput. Phys.*, 461 (2022), p. 111215, <https://doi.org/10.1016/j.jcp.2022.111215>.
 - [19] L. FORMAGGIA AND F. NOBILE, *A stability analysis for the Arbitrary Lagrangian Eulerian formulation with finite elements*, *East-West J. Numer. Math.*, 7 (1999).
 - [20] H. GARCKE, R. NÜRNBERG, AND Q. ZHAO, *Structure-preserving discretizations of two-phase Navier–Stokes flow using fitted and unfitted approaches*, *J. Comput. Phys.*, 489 (2023), p. 112276, <https://doi.org/10.1016/j.jcp.2023.112276>.
 - [21] W. HAO, P. SUN, J. XU, AND L. ZHANG, *Multiscale and monolithic arbitrary Lagrangian–Eulerian finite element method for a hemodynamic fluid–structure interaction problem involving aneurysms*, *J. Comput. Phys.*, 433 (2021), p. 110181, <https://doi.org/10.1016/j.jcp.2021.110181>.
 - [22] T. HUGHES, W. LIU, AND T. ZIMMERMAN, *Lagrangian Eulerian finite elements formulation for viscous flows*, *Comput. Methods Appl. Mech. Engrg.*, 21 (1981), pp. 329–349, [https://doi.org/10.1016/0045-7825\(81\)90049-9](https://doi.org/10.1016/0045-7825(81)90049-9).
 - [23] W. LENG, C.-S. ZHANG, P. SUN, B. GAO, AND J. XU, *Numerical simulation of an immersed rotating structure in fluid for hemodynamic applications*, *J. Comput. Sci.*, 30 (2019), pp. 79–89, <https://doi.org/10.1016/j.jocs.2018.11.010>.
 - [24] M. LENOIR, *Optimal isoparametric finite elements and error estimates for domains involving curved boundaries*, *SIAM J. Numer. Anal.*, 23 (1986), pp. 562–580, <https://doi.org/10.1137/0723036>.
 - [25] C. MICHAILIDES AND D. ANGELIDES, *Modeling of energy extraction and behavior of a flexible floating breakwater*, *Appl. Ocean Res.*, 35 (2012), pp. 77–94, <https://doi.org/10.1016/j.apor.2011.11.004>.
 - [26] T. NGO, P. MENDIS, A. GUPTA, AND J. RAMSAY, *Blast loading and blast effects on structures – an overview*, *Electron. J. Struct. Eng.*, 7 (2007), pp. 76–91, <https://doi.org/10.56748/ejse.671>.
 - [27] T. RICHTER, *Fluid-Structure Interactions: Models, Analysis and Finite Elements*, Lecture Notes in Computational Science and Engineering, Springer International Publishing, 2017, <https://doi.org/10.1007/978-3-319-63970-3>.
 - [28] M. SOULI, A. OUAHSINE, AND L. LEWIN, *ALE formulation for fluid–structure interaction problems*, *Comput. Methods Appl. Mech. Engrg.*, 190 (2000), pp. 659–675, [https://doi.org/10.1016/S0045-7825\(99\)00432-6](https://doi.org/10.1016/S0045-7825(99)00432-6).
 - [29] P. SUN, W. LENG, C.-S. ZHANG, R. LAN, AND J. XU, *ALE method for a rotating structure immersed in the fluid and its application to the artificial heart pump in hemodynamics*, in *Comput. Sci. – ICCS 2018, Lecture Notes in Computer Science*, Springer International Publishing, 2018, pp. 9–23, https://doi.org/10.1007/978-3-319-93713-7_1.
 - [30] T. TEZDUYAR, S. ALIABADI, M. BEHR, A. JOHNSON, V. KALRO, AND M. LITKE, *Flow simulation and high performance computing*, *Comput. Mech.*, 18 (1996), pp. 397–412, <https://doi.org/10.1007/BF00350249>.
 - [31] T. E. TEZDUYAR, M. BEHR, AND J. LIOU, *A new strategy for finite element computations involving moving boundaries and interfaces—The deforming-spatial-domain/space-time procedure: I. The concept and the preliminary numerical tests*, *Comput. Methods Appl. Mech. Eng.*, 94 (1992), pp. 339–351, [https://doi.org/10.1016/0045-7825\(92\)90059-S](https://doi.org/10.1016/0045-7825(92)90059-S).
 - [32] S. W. WALKER, *The Shapes of Things: A Practical Guide to Differential Geometry and the Shape Derivative*, SIAM, 2015.
 - [33] K. YANG, P. SUN, L. WANG, J. XU, AND L. ZHANG, *Modeling and simulations for fluid and rotating structure interactions*, *Comput. Methods Appl. Mech. Eng.*, 311 (2016), pp. 788–814, <https://doi.org/10.1016/j.cma.2016.09.020>.